Received: 3 May 2022 | Revised: 17 February 2023 | Accepted: 12 March 2023

DOI: 10.1002/acs.3585

RESEARCH ARTICLE

WILEY

Range observer-based formation control for heterogeneous spatial underactuated vehicle networks

Bo Wang | **Sergey Nersesov** | **Hashem Ashrafiuon**

Department of Mechanical Engineering, Villanova University, Villanova, Pennsylvania, USA

Correspondence
Hashem Ashrafiuon, Department of Mechanical Engineering, Villanova University, Villanova, PA 19085, USA.
Email: hashem.ashrafiuon@villanova.edu

Funding information
Office of Naval Research, Grant/Award Number: N00014-19-1-2255

Abstract

In this work, we solve the distributed formation control problem for heterogeneous spatial underactuated vehicle networks subject to switching topologies. We consider the spatial rigid body model of underwater and aerial vehicles with one translational actuator for propulsion and three rotational actuators, without any simplification. A distributed finite-time sliding mode observer is designed to estimate the ranges between vehicles based on the bearing angles, and thus, the control design does not require relative position or distance measurements. A coordinate transformation is proposed to define continuous reference velocity trajectories under switching topologies. Then, based on the cascade structure, a distributed formation protocol is presented which guarantees the global asymptotic convergence for the closed-loop system. The formation controller has a simple structure, requires only neighbor-to-neighbor information exchange, and all the measurements may be obtained using simple onboard sensors. Numerical simulations for a group of heterogeneous spatial underactuated vehicles including autonomous underwater vehicles and quadrotors are presented.

KEYWORDS

formation control, heterogeneous multi-agent systems, range estimation, spatial underactuated vehicles, switching topologies

1 | INTRODUCTION

1.1 | Motivation

The cooperative control problem of multiple autonomous vehicles has received great attention in the past two decades because of its significant civilian, industrial, and military applications. The advantages of multi-vehicle systems over single vehicles include higher efficiency, robustness, and flexibility.[1] Numerous cooperative control strategies have been proposed in the literature for autonomous vehicles modeled by single-integrator dynamics,[2-4] double-integrator dynamics,[5,6] and (fully-actuated) Euler-Lagrangian (EL) systems.[7,8] See Reference 9 for a detailed review of the early literature.

However, most of the vehicles in practical applications are *underactuated*. That is, the vehicle has fewer independent actuators than its degrees of freedom (DOF), for instance, wheeled mobile robots, marine surface vessels, quadrotors, and so forth. The motion control of underactuated mechanical systems is far more complicated than the control of fully-actuated systems. A key characteristic of underactuated mechanical systems is that they are not feedback

linearizable, that is, they cannot be transformed into integrator dynamics via preliminary feedback. As a consequence, the approaches developed for integrator dynamics[2-6] and for fully-actuated EL systems[7,8] cannot be directly applied to underactuated vehicle networks.

Furthermore, a multi-vehicle system usually contains different types of vehicles. For instance, a combination of ground, marine, and aerial vehicles can be used for military operations to increase the striking force from multiple sources. Thus, it is more practical if a group of vehicles can cooperate with each other regardless of the structures of their dynamic models. To address this problem, several analysis and design approaches have been presented in recent years for heterogeneous multi-agent systems such as for heterogeneous linear systems[10] and for heterogeneous nonlinear systems in the normal form.[11] In spite of this, there have not been many efforts to develop cooperative control approaches that can be applied to *heterogeneous underactuated* multi-agent systems.

Moreover, an important theme in multi-agent control systems is *decentralization*, namely, *distributed algorithms* where each agent senses the *relative* configuration variables of its neighbors with respect to its *local* coordinate system.[12] In other words, distributed control schemes do not require a global coordinator where measurements are performed by onboard sensors and are significantly more scalable and robust compared to the centralized ones, which is extremely useful in the Global Positioning System (GPS)-denied environments. For these controllers, cameras and inertial measurement units (IMUs) are usually the preferred onboard sensors compared to LiDARs due to lower weight and cost. These sensors can measure bearing angles, postures, velocities, and accelerations, while the range between vehicles cannot be directly measured by these sensors. Hence, the range or relative position must be estimated. Another requirement for distributed cooperative control of multi-agent systems is communication.[3] Switching communication topologies and communication delays are common in a communication network, and thus, they should be considered when designing a controller.

1.2 | Related works

As a prelude to cooperative control of heterogeneous underactuated vehicle networks, a general approach is needed to control a class of underactuated vehicles. In Reference 13, a trajectory tracking control framework was proposed for generic planar vehicles, which is applicable to wheeled mobile robots, surface vessels, and planar vertical take-off and landing (PVTOL) aircraft. Using similar ideas, the trajectory tracking control problem was solved for generic spatial vehicles with one degree of underactuation in Reference 14, and spatial vehicles with two degrees of underactuation in Reference 15.

Formation control of planar underactuated vehicle networks has been addressed by several researchers. Jin[16] presented a finite-time fault-tolerant formation control law for heterogeneous underactuated surface vessels with line-of-sight range and angle constraints. Yoo and Park[17] proposed a predefined performance control approach for distributed containment control of heterogeneous underactuated surface vessels. Li et al.[18] solved the formation control problem for a class of discrete-time heterogeneous nonlinear multi-agent systems and applied it to ground multi-vehicle systems. In our previous work,[19] a simultaneous formation stabilization and tracking control approach was proposed for heterogeneous planar underactuated vehicle networks based on the persistence of excitation. Time-varying formation control laws and distributed obstacle avoidance algorithms were presented in References 20,21 for heterogeneous planar underactuated multi-vehicle systems.

There are plenty of works on cooperative control of *homogeneous* spatial underactuated vehicle networks in the literature as well. For example, a coordination control law was proposed in Reference 22 for a group of quadrotors which guarantees no collision between them. Later, a finite-time formation control law was proposed in Reference 23 for a group of quadrotors based on a non-smooth backstepping design. In Reference 24, based on finite-time state observers, a robust coordinated tracking controller was developed for multiple quadrotors with external disturbances. A robust formation tracking control design was presented in the work of Liu et al.[25] for multiple quadrotors subject to switching topologies. Recently, a robust consensus control algorithm was proposed in Reference 26 based on backstepping techniques and applied to a group of quadrotors subject to connectivity and collision-avoidance constraints. In Reference 27, an adaptive formation control method was proposed for a class of networked quadrotor aircraft with partially bounded and state-dependent perturbations based on adaptive technique and Lyapunov theory. In Reference 28, a neural network-based formation controller was presented for underactuated autonomous underwater vehicles (AUVs) under environmental disturbances in three-dimensional space. Using a simplified 5-DOF model, a filter-backstepping-based neural adaptive formation controller was proposed for networked AUV systems in Reference 29.

However, cooperative control of *heterogeneous* spatial underactuated vehicle networks has not been sufficiently addressed in the literature. In the work of Zhang et al.,[30] the formation–containment control problem was considered for heterogeneous underactuated AUVs in three-dimensional space based on a simplified 5-DOF model. In the works of Mu et al.,[31,32] an integral sliding mode control law and a linear quadratic regulation (LQR) consensus protocol were proposed for heterogeneous multi-vehicle systems consisting of quadrotors and wheeled mobile robots based on the linearized models. Recently, in Reference 33, a coordinated trajectory tracking controller was developed based on cascaded system theory and Lyapunov analysis for the marine aerial-surface heterogeneous system composed of a quadrotor and a (fully-actuated) surface vehicle. Nevertheless, in the above-mentioned works,[30-33] the vehicle models in the heterogeneous networks are either simplified, linearized, or partially assumed to be fully actuated.

1.3 | Main contributions

This work is the outgrowth of our previous works[19-21] on cooperative control for heterogeneous *planar* underactuated multi-vehicle systems. In this work, we focus on the distributed formation control problem for heterogeneous networks of *spatial* underactuated vehicles with two degrees of underactuation. The main contributions of this work are summarized as follows:

1. We solve the distributed formation control problem for a class of *heterogeneous* spatial underactuated vehicle networks with a directed communication graph. We consider a generic spatial vehicle model with two degrees of underactuation, which includes underwater and aerial vehicles with one translational actuator and three rotational actuators, without any simplification. For each vehicle, the dynamics are decoupled into two parts: the attitude control subsystem and the position control subsystem. Based on the cascaded structure, the formation controller considers the nonlinearity and heterogeneity of the systems and guarantees the global asymptotic convergence for the closed-loop system state.
2. The proposed formation control protocol works even when the vehicle network is subject to *switching topologies*. It is shown that switching topologies do not matter if the communication graph contains a directed spanning tree. Furthermore, the proposed control law is *robust to communication delays*. To be precise, we present a generalized Slotine-Li controller for distributed consensus of arbitrary order multi-agent systems, where a two-step control design procedure is applied, similar to the original Slotine-Li controller[34] (or sliding mode control design). First, a reference velocity trajectory that contains the position error information is defined such that, if the velocity converges to the reference velocity, the position error will also converge to zero. Next, a controller is designed to stabilize the (reduced-order) velocity error system. However, the reference velocity trajectory in this work is defined by integration, which is different from the original Slotine-Li controller. As a result, the reference velocity trajectory is always continuous due to the integral action even under switching topologies. Based on the generalized Slotine-Li transformation, the control design is reduced to stabilize an integrator chain.
3. Instead of requiring the relative positions, the proposed control protocol requires the *bearing angle information* of the neighbor vehicles. Using the distributed sliding mode observers, the ranges between the vehicle and its neighbors are estimated in finite time based on the bearing, attitude, and local velocity measurements. It should be emphasized that the bearing angles of the neighbors can be easily measured by onboard monocular cameras, which are much cheaper and lighter than LiDARs. Furthermore, the proposed distributed control law requires only neighbor-to-neighbor information exchange, and all the measurements are performed by onboard sensors. The controller also has a simple structure, and thus, is practical and easy to implement.

Compared with existing results in the literature and in contrast to existing controllers in References 22-27, which are applicable only to *homogeneous* quadcopter networks, the approach proposed in this article can be applied to *heterogeneous* spatial underactuated vehicle networks. In contrast to the existing methods in References 30-33, the approach proposed in this article does not simplify the model and considers the full nonlinear vehicle dynamics. In contrast to the existing methods in References 16-21, the proposed approach is robust to *switching topologies* and *communication delays*. In contrast to the traditional bearing-based formation methods in References 35-37, where the target formation is required to be *rigid* and the group leaders are required to move at a common *constant* velocity, the approach proposed in this article only requires the existence of *directed spanning tree* topology.

1.4 | Outline

The rest of the paper is organized as follows. Preliminaries and problem formulation are given in Section 2. Section 3 presents the finite-time sliding mode observer design for range estimation. In Section 4, we present the generalized Slotine-Li controller, formation control design, and stability analysis. Numerical simulations are presented in Section 5. The concluding remarks are provided in Section 6.

2 | PRELIMINARIES AND PROBLEM STATEMENT

2.1 | Notations

Let $\mathbb{R}^n$ represent the n-dimensional real vector space; $|\cdot|$ the Euclidean norm of vectors in $\mathbb{R}^n$; $\mathbb{R}_{\geq 0}$ the set of all non-negative real numbers; $\mathbb{Z}_{\geq 0}$ the set of all non-negative integers; $I_n \in \mathbb{R}^{n\times n}$ the identity matrix; $\mathbb{S}^n$ the n-sphere, that is, $\mathbb{S}^n = \{x \in \mathbb{R}^{n+1} : |x| = 1\}$; SO(3) the special orthogonal group and $\mathfrak{so}(3)$ the associated Lie algebra; s the differential operator, i.e., $s = \frac{\mathrm{d}}{\mathrm{d}t}[\cdot]$. Given $a = [a_1, a_2, a_3]^\top \in \mathbb{R}^3$, we define the operator $(\cdot)_\times$ as

$$a_\times = \begin{bmatrix} 0 & -a_3 & a_2 \\ a_3 & 0 & -a_1 \\ -a_2 & a_1 & 0 \end{bmatrix} \in \mathfrak{so}(3). \tag{1}$$

We use the abbreviation $s_{(\cdot)} = \sin(\cdot)$, $c_{(\cdot)} = \cos(\cdot)$, and $t_{(\cdot)} = \tan(\cdot)$. For multi-agent systems considered in this paper, we use the bold and non-italicized subscript **i** to denote the index of an agent.

2.2 | Model of spatial underactuated vehicles

Consider a network of N heterogeneous spatial underactuated vehicles, where the agents are numbered $\mathbf{i} = 1, \ldots, N$ with **1** representing the group leader and **2, … ,N** representing the followers. Each vehicle is modeled as a 6-DOF rigid body moving in three-dimensional Euclidean space. Let $\{\mathcal{I}\}$ denote an earth-fixed inertial frame, and $\{\mathcal{B}_\mathbf{i}\}$ the body-fixed frame attached to vehicle **i**, where the origin is located at the center of mass of the vehicle, as shown in Figure 1. The position of vehicle **i** in the earth-fixed frame $\{\mathcal{I}\}$ is represented by $\xi_\mathbf{i} = [x_\mathbf{i}, y_\mathbf{i}, z_\mathbf{i}]^\top$, and the attitude is represented by the Euler angles $\eta_\mathbf{i} = [\phi_\mathbf{i}, \theta_\mathbf{i}, \psi_\mathbf{i}]^\top$ of $\{\mathcal{B}_\mathbf{i}\}$ relative to $\{\mathcal{I}\}$, where $\phi_\mathbf{i}, \theta_\mathbf{i}, \psi_\mathbf{i}$ represent the roll, pitch, and yaw angles, respectively. Let $v_\mathbf{i} = [v_{x\mathbf{i}}, v_{y\mathbf{i}}, v_{z\mathbf{i}}]^\top$ and $\omega_\mathbf{i} = [\omega_{x\mathbf{i}}, \omega_{y\mathbf{i}}, \omega_{z\mathbf{i}}]^\top$ denote the linear and angular velocity vectors of vehicle **i**, respectively, resolved

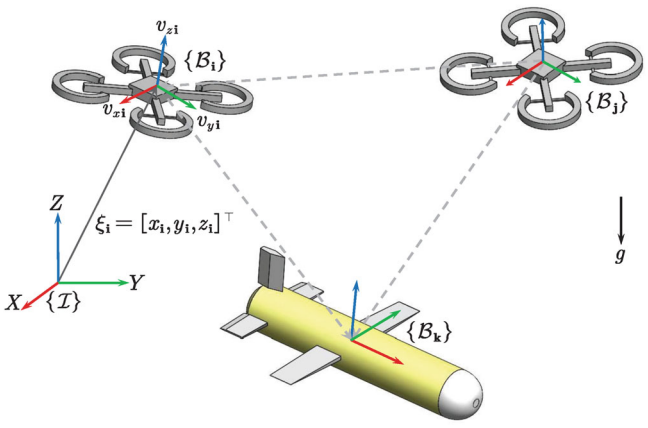

FIGURE 1 Illustration of the leader-follower formation of heterogeneous spatial underactuated vehicle networks, where the network consists of two quadrotors and an AUV.

in its body-fixed frame. The kinematics of vehicle $\mathbf{i}$ is described by Reference 38

$$\begin{bmatrix} \dot{\xi}_{\mathbf{i}} \\ \dot{\eta}_{\mathbf{i}} \end{bmatrix} = \begin{bmatrix} R(\eta_{\mathbf{i}}) & 0 \\ 0 & T(\eta_{\mathbf{i}}) \end{bmatrix} \begin{bmatrix} v_{\mathbf{i}} \\ \omega_{\mathbf{i}} \end{bmatrix} \tag{2}$$

where $R(\cdot) \in \mathrm{SO}(3)$ is the rotation matrix parameterized by Euler angles $\eta = [\phi, \theta, \psi]^\top$, that is,

$$R(\eta) = \begin{bmatrix} c_\theta c_\psi & s_\phi s_\theta c_\psi - c_\phi s_\psi & c_\phi s_\theta c_\psi + s_\phi s_\psi \\ c_\theta s_\psi & s_\phi s_\theta s_\psi + c_\phi c_\psi & c_\phi s_\theta s_\psi - s_\phi c_\psi \\ -s_\theta & s_\phi c_\theta & c_\phi c_\theta \end{bmatrix}, \tag{3}$$

and the matrix $T(\cdot)$ is given by

$$T(\eta) = \begin{bmatrix} 1 & s_\phi t_\theta & c_\phi t_\theta \\ 0 & c_\phi & -s_\phi \\ 0 & \frac{s_\phi}{c_\theta} & \frac{c_\phi}{c_\theta} \end{bmatrix}. \tag{4}$$

Note that the matrix $T(\eta)$ becomes singular when $\theta = \pm\pi/2$, and thus, we restrict the use of Euler angles to $|\phi_{\mathbf{i}}| < \pi/2$ and $|\theta_{\mathbf{i}}| < \pi/2$ to avoid aggressive maneuvers and singularity.[15]

We consider the spatial vehicle model with two degrees of underactuation. More precisely, we assume that each vehicle has only one control thrust (force) and three control torques. The dynamic Euler-Lagrangian model of vehicle $\mathbf{i}$ can be written as

$$\begin{bmatrix} m_{\mathbf{i}} I_3 & 0 \\ 0 & I_{\mathbf{i}} \end{bmatrix} \begin{bmatrix} \dot{v}_{\mathbf{i}} \\ \dot{\omega}_{\mathbf{i}} \end{bmatrix} + \begin{bmatrix} \omega_{\mathbf{i}} \times (m_{\mathbf{i}} v_{\mathbf{i}}) \\ \omega_{\mathbf{i}} \times (I_{\mathbf{i}} \omega_{\mathbf{i}}) \end{bmatrix} + \begin{bmatrix} D_{v\mathbf{i}} & 0 \\ 0 & D_{\omega\mathbf{i}} \end{bmatrix} \begin{bmatrix} v_{\mathbf{i}} \\ \omega_{\mathbf{i}} \end{bmatrix} = \begin{bmatrix} F_{\mathbf{i}} + R(\eta_{\mathbf{i}})^\top G_{\mathbf{i}} \\ \tau_{\mathbf{i}} \end{bmatrix}, \tag{5}$$

where $m_{\mathbf{i}}$ is the total mass of the vehicle; $I_{\mathbf{i}} \in \mathbb{R}^{3\times3}$ is the diagonal inertia matrix; $D_{v\mathbf{i}}$, $D_{\omega\mathbf{i}} \in \mathbb{R}^{3\times3}$ are constant, positive semi-definite damping matrices; $F_{\mathbf{i}}$ is the control thrust force; $G_{\mathbf{i}} = [0, 0, G_{z\mathbf{i}}]^\top$ is the total force of gravity and the buoyancy (if exists); $\tau_{\mathbf{i}} = [\tau_{\phi\mathbf{i}}, \tau_{\theta\mathbf{i}}, \tau_{\psi\mathbf{i}}]^\top$ is the control torque vector. Note that the vehicle system (2)–(5) is in the Euler-Lagrangian form. The system is underactuated because it has six DOF, that is, three translational DOF and three rotational DOF, however, it only has four independent control inputs, that is, one control thrust force, and three control torques. Without any loss of generality, we assume that the control thrust is in the direction of one of the three body-fixed axes, that is, $F_{\mathbf{i}} = [F_{x\mathbf{i}}, 0, 0]^\top$, $F_{\mathbf{i}} = [0, F_{y\mathbf{i}}, 0]^\top$, or $F_{\mathbf{i}} = [0, 0, F_{z\mathbf{i}}]^\top$. It should be noted that the full nonlinear vehicle model (2)–(5) can represent a wide class of spatial underactuated vehicles including AUVs ($F_{\mathbf{i}} = [F_{x\mathbf{i}}, 0, 0]^\top$) and quadrotors ($F_{\mathbf{i}} = [0, 0, F_{z\mathbf{i}}]^\top$).[15]

Taking time derivative of (2), substituting (5), and using the properties that $R(\eta_{\mathbf{i}})^\top = R(\eta_{\mathbf{i}})^{-1}$, $\dot{R}(\eta_{\mathbf{i}}) = R(\eta_{\mathbf{i}})(\omega_{\mathbf{i}})_\times$, and $(\omega_{\mathbf{i}})_\times v_{\mathbf{i}} = \omega_{\mathbf{i}} \times v_{\mathbf{i}}$, we obtain the equations of motion in the earth-fixed frame:

$$\ddot{\xi}_{\mathbf{i}} = R(\eta_{\mathbf{i}}) u_{\mathbf{i}} + \frac{G_{\mathbf{i}}}{m_{\mathbf{i}}} - D_{\xi\mathbf{i}}(\eta_{\mathbf{i}}) \dot{\xi}_{\mathbf{i}}, \tag{6}$$

$$\ddot{\eta}_{\mathbf{i}} = \tilde{\tau}_{\mathbf{i}}, \tag{7}$$

where $D_{\xi\mathbf{i}}(\eta_{\mathbf{i}}) = (1/m_{\mathbf{i}}) R(\eta_{\mathbf{i}}) D_{v\mathbf{i}} R(\eta_{\mathbf{i}})^\top$; $u_{\mathbf{i}} = F_{\mathbf{i}}/m_{\mathbf{i}}$ and $\tilde{\tau}_{\mathbf{i}} = [\tilde{\tau}_{\phi\mathbf{i}}, \tilde{\tau}_{\theta\mathbf{i}}, \tilde{\tau}_{\psi\mathbf{i}}]^\top = \dot{T}(\eta_{\mathbf{i}}) \omega_{\mathbf{i}} - T(\eta_{\mathbf{i}}) I_{\mathbf{i}}^{-1} [\omega_{\mathbf{i}} \times (I_{\mathbf{i}} \omega_{\mathbf{i}}) + D_{\omega\mathbf{i}} \omega_{\mathbf{i}} - \tau_{\mathbf{i}}]$ are the new control inputs. Note that $u_{\mathbf{i}} = [u_{x\mathbf{i}}, 0, 0]^\top, [0, u_{y\mathbf{i}}, 0]^\top$, or $[0, 0, u_{z\mathbf{i}}]^\top$ according to the specific configuration of the thrust actuator, where $u_{(\cdot)\mathbf{i}} = F_{(\cdot)\mathbf{i}}/m_{\mathbf{i}}$.

2.3 | Notions from graph theory

The information exchange among the N vehicles is modeled as a time-varying directed graph $\mathcal{G}(t) = (\mathcal{V}, \mathcal{E}(t), \mathcal{A}(t))$, where each vehicle is considered as a node in the graph, that is, the vortex set $\mathcal{V} = \{\mathbf{1}, \ldots, \mathbf{N}\}$; $\mathcal{E}(t) \subseteq \mathcal{V} \times \mathcal{V}$ is the edge set;

and $\mathcal{A}(t) \in \mathbb{R}^{N\times N}$ is the weighted adjacency matrix.[1] The set of neighboring nodes with edges connected to the node $\mathbf{i}$ is denoted by $\mathcal{N}_{\mathbf{i}}(t) = \{\mathbf{j} \in \mathcal{V} : (\mathbf{i},\mathbf{j}) \in \mathcal{E}_t\}$, where $(\mathbf{i},\mathbf{j})$ represents that node $\mathbf{i}$ obtains information from node $\mathbf{j}$ via communication. The weighted adjacency matrix $\mathcal{A}(t) = [a_{\mathbf{ij}}(t)]$ is defined as $a_{\mathbf{ij}}(t) > 0$ if $\mathbf{j} \in \mathcal{N}_{\mathbf{i}}(t)$ and $a_{\mathbf{ij}}(t) = 0$ otherwise, for each $t \geq 0$. The physical meaning of the weighting coefficients $a_{\mathbf{ij}}(t)$ is in the different levels of importance of the agent neighbors' information states. We assume that the graph $\mathcal{G}(t)$ has no self-loop or loop for each $t \geq 0$, and that the group leader does not receive any communication from other nodes. For more details on algebraic graph theory, see References 1,9.

The directed graph $\mathcal{G}(t)$ considered in this paper is switching in formation control of the heterogeneous multi-vehicle systems. We make the following assumption on the adjacency matrix $\mathcal{A}(t)$.

Assumption 1. (i) $\mathcal{A}(t)$ is is piecewise continuous for all $t \geq 0$; (ii) each nonzero entry $a_{\mathbf{ij}}(t)$ is bounded, that is, there exist positive constants $\underline{a}, \bar{a}$ such that $\underline{a} < a_{\mathbf{ij}}(t) < \bar{a}$; (iii) Let $t_0 = 0$ and let $t_1, t_2, \ldots$ be the switching times for $\mathcal{A}(t)$. The directed switching graph $\mathcal{G}(t)$ has a directed spanning tree across each interval $[t_i, t_{i+1})$, $\forall i \in \mathbb{Z}_{\geq 0}$, that is, there exists at least one directed path starting from the group leader to any other node in the network.

2.4 | Problem statement

The objective of formation control is to design a distributed controller for each follower agent such that it coordinates its motion relative to its neighbors, and the network asymptotically converges to a predefined geometric pattern. The desired geometric pattern of the vehicle network in terms of spatial positions is defined by a set of constant position offset vectors $\{d_{\mathbf{ij}} = [d^x_{\mathbf{ij}}, d^y_{\mathbf{ij}}, d^z_{\mathbf{ij}}]^\top \in \mathbb{R}^3 : \mathbf{i},\mathbf{j} \in \mathcal{V}, \mathbf{i} \neq \mathbf{j}\}$. To be more specific, under Assumption 1, we will design a controller for each follower (6) and (7) without global position measurements or relative range measurements such that: (i) the state trajectories of the closed-loop system are bounded for all $t \geq 0$; (ii) all the vehicles in the network can maintain a prescribed formation in the sense that for all $\mathbf{i} \in \mathcal{V}$,

$$\lim_{t\to+\infty} \sum_{\mathbf{j}\in\mathcal{N}_{\mathbf{i}}(t)} |\xi_{\mathbf{i}}(t) - \xi_{\mathbf{j}}(t) - d_{\mathbf{ij}}| = 0. \tag{8}$$

In this paper, we choose constant offset vectors $d_{\mathbf{ij}}$ for simplicity of exposition, and the results can be extended to address smooth time-varying formation geometry.

2.5 | Technical lemmas

The following lemmas are needed for developing the main results of the paper.

Lemma 1 *(*Reference 1, Thm. 3.11*). Consider the single-integrator dynamics $\dot{x}_{\mathbf{i}} = u_{\mathbf{i}}$, where $x_{\mathbf{i}} \in \mathbb{R}^n$, $\mathbf{i} = 1, \ldots, N$ with the network communication graph satisfying Assumption 1. Then, under the control law*

$$u_{\mathbf{i}} = \frac{1}{\Xi_{\mathbf{i}}(t)} \sum_{\mathbf{j}\in\mathcal{N}_{\mathbf{i}}(t)} a_{\mathbf{ij}}(t) \left[\dot{x}_{\mathbf{j}} - \alpha(x_{\mathbf{i}} - x_{\mathbf{j}})\right], \quad \mathbf{i} = 1, \ldots, N, \tag{9}$$

where $\Xi_{\mathbf{i}}(t) = \sum_{\mathbf{j}\in\mathcal{N}_{\mathbf{i}}(t)} a_{\mathbf{ij}}(t)$, and $\alpha > 0$ is a constant, the consensus tracking problem is solved.

Lemma 2 *(*Swapping lemma[39]*). For continuous differentiable signals $x, y : \mathbb{R}_{\geq 0} \to \mathbb{R}$, the following holds for any $\alpha > 0$*

$$\frac{\alpha}{s+\alpha}[xy] = y\frac{\alpha}{s+\alpha}[x] - \frac{1}{s+\alpha}\left[\dot{y}\frac{\alpha}{s+\alpha}[x]\right]. \tag{10}$$

3 | RANGE OBSERVER DESIGN

In this section, we present a distributed finite-time sliding mode observer for range estimation among spatial vehicles based on the relative bearing, attitude, and local velocity measurements in the formation. Observer design for the range

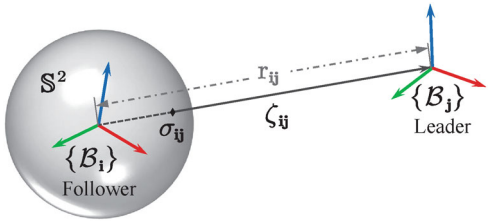

FIGURE 2 Illustration of the bearing and the range of leader **j** with respect to follower **i**.

estimation problem between a spatial robot and a *static* feature point is presented in References 40,41. Compared to the observers presented in Reference 41, the sliding mode observer proposed in this work can be applied to moving objects, avoids open-loop integration, and guarantees finite-time estimation.

We consider a pair of agents (**i**,**j**), where agent **j** is the leader and agent **i** is the follower, as shown in Figure 2. In the body-fixed frame $\{\mathcal{B}_i\}$, the relative position vector of agent **j** is denoted by

$$\zeta_{ij} = R(\eta_i)^\top(\xi_j - \xi_i). \tag{11}$$

We assume that the measurable signal is the bearing angle of vehicle **j** in the body-fixed frame $\{\mathcal{B}_i\}$. In other words, we measure the projection of ζ_{ij} on the unit sphere centered at the origin of $\{\mathcal{B}_i\}$, that is,

$$\sigma_{ij} = \frac{\zeta_{ij}}{|\zeta_{ij}|} \in \mathbb{S}^2. \tag{12}$$

The bearing angle σ_{ij} is well defined for all $|\zeta_{ij}| \neq 0$. The problem is to estimate the range $r_{ij} = |\zeta_{ij}|$ based on the bearing angle σ_{ij}, the attitude, and the velocity measurements.

To start with, we write the error dynamics in the body-fixed frame $\{\mathcal{B}_i\}$. Note that

$$\dot{\overbrace{|\zeta_{ij}|^2}} = 2|\zeta_{ij}|\dot{\overbrace{|\zeta_{ij}|}} = \dot{\overbrace{\zeta_{ij}^\top\zeta_{ij}}} = 2\zeta_{ij}^\top\dot{\zeta}_{ij} = 2r_{ij}\dot{r}_{ij}, \tag{13}$$

and $\dot{r}_{ij} = \sigma_{ij}^\top\dot{\zeta}_{ij}$. Taking time derivative of (11), and substituting (2), we obtain

$$\dot{r}_{ij} = \sigma_{ij}^\top\left[R(\eta_i)^\top R(\eta_j)v_j - v_i\right] = \sigma_{ij}^\top w_{ij}, \tag{14}$$

where $w_{ij} = R(\eta_i)^\top R(\eta_j)v_j - v_i$, and we used the fact that the matrix $(\omega_i)_\times$ is skew-symmetric. Taking time derivative of (12), we have

$$\dot{\sigma}_{ij} = -(\omega_i)_\times\sigma_{ij} + \frac{1}{r_{ij}}\left(I_3 - \sigma_{ij}\sigma_{ij}^\top\right)w_{ij}. \tag{15}$$

Multiplying by r_{ij} and applying the stable filter $\alpha/(s+\alpha)$ with $\alpha > 0$ to both sides of (15) yields

$$\frac{\alpha}{s+\alpha}[r_{ij}\dot{\sigma}_{ij}] = \frac{\alpha}{s+\alpha}\left[-r_{ij}(\omega_i)_\times\sigma_{ij}\right] + \frac{\alpha}{s+\alpha}\left[\left(I_3 - \sigma_{ij}\sigma_{ij}^\top\right)w_{ij}\right]. \tag{16}$$

Applying Lemma 2, the left-hand side of (16) becomes

$$\alpha G_2[r_{ij}\dot{\sigma}_{ij}] = r_{ij}G_1[\sigma_{ij}] - G_2\left[\sigma_{ij}^\top w_{ij}G_1[\sigma_{ij}]\right]. \tag{17}$$

where $G_1(s) = \alpha s/(s+\alpha)$ and $G_2(s) = 1/(s+\alpha)$. Substituting (17) into (16) and applying Lemma 2 again, we obtain

$$r_{ij}\Phi_{ij} = G_2\left[\sigma_{ij}^\top w_{ij}\Phi_{ij}\right] + \alpha G_2\left[(I_3 - \sigma_{ij}\sigma_{ij}^\top)w_{ij}\right], \tag{18}$$

where $\Phi_{ij} = G_1[\sigma_{ij}] + \alpha G_2\left[(\omega_i)_\times\sigma_{ij}\right]$ is a continuous measurable signal.

Proposition 1. *Consider the dynamics (14) and (15) with input w_{ij}. The sliding mode observer*

$$\dot{\hat{r}}_{ij} = \sigma_{ij}^{\top} w_{ij} - \gamma sign\left\{\Phi_{ij}^{\top}\left(\Phi_{ij}\hat{r}_{ij} - G_2\left[\sigma_{ij}^{\top} w_{ij}\Phi_{ij}\right] - \alpha G_2\left[(I_3 - \sigma_{ij}\sigma_{ij}^{\top})w_{ij}\right]\right)\right\} \tag{19}$$

$$\hat{\zeta}_{ij} = \sigma_{ij}\hat{r}_{ij} \tag{20}$$

with $\gamma > 0$ provides a globally finite-time convergent estimate to the relative position error ζ_{ij}, that is, there exists $T_r > 0$ such that $\hat{\zeta}_{ij}(t) = \zeta_{ij}(t)$ for all $t \geq T_r$, if the signal $\Phi_{ij}^{\top}$ is persistently exciting (PE), that is, there exist $\mu, T > 0$ such that

$$\int_t^{t+T} \Phi_{ij}(s)^{\top}\Phi_{ij}(s) \geq \mu, \quad \forall t \geq 0. \tag{21}$$

Proof. Define the estimation error $\tilde{r}_{ij} = \hat{r}_{ij} - r_{ij}$. Substituting (18) into (19), the observation error dynamics are given by

$$\dot{\tilde{r}}_{ij} = -\gamma \text{sign}\left(\Phi_{ij}^{\top}\Phi_{ij}\right)\text{sign}\left(\tilde{r}_{ij}\right). \tag{22}$$

Consider the Lyapunov candidate $V(\tilde{r}_{ij}) = |\tilde{r}_{ij}|$, where its derivative is calculated as

$$\dot{V} = \begin{cases} -\gamma \text{sign}\left(\Phi_{ij}^{\top}\Phi_{ij}\right) & , \ \tilde{r}_{ij} \neq 0 \\ 0 & , \ \tilde{r}_{ij} = 0. \end{cases} \tag{23}$$

It should be noted that the function V is continuous, and (23) implies that the time derivative of V along trajectories is non-increasing. For each $\tilde{r}_{ij}(0) \neq 0$, we have, along trajectories, $\dot{V}(\tilde{r}_{ij}(t)) = -\gamma$, if $\Phi_{ij}(t)^{\top}\Phi_{ij}(t) > 0$, and $\dot{V}(\tilde{r}_{ij}(t)) = 0$, if $\Phi_{ij}(t)^{\top}\Phi_{ij}(t) = 0$. Due to the PE condition (21) and the continuity of $\Phi_{ij}(t)$, for each time interval $[t, t+T]$, the measure of the set $\{s \in [t, t+T] : \Phi_{ij}(s)^{\top}\Phi_{ij}(s) \geq \mu/T\}$ must be (strictly) larger than zero. Define $l_{[a,b]}$ as the measure of the set $\{s \in [a, b] : \Phi_{ij}(s)^{\top}\Phi_{ij}(s) > 0\}$. We have, for all $t \geq 0$,

$$l_{[t,t+T]} = \text{meas}\{s \in [t, t+T] : \Phi_{ij}(s)^{\top}\Phi_{ij}(s) > 0\} > \text{meas}\{s \in [t, t+T] : \Phi_{ij}(s)^{\top}\Phi_{ij}(s) \geq \mu/T\} > 0. \tag{24}$$

Integrating both sides of (23) along trajectories yields $V(\tilde{r}_{ij}(t)) = V(\tilde{r}_{ij}(0)) - \gamma l_{[0,t]}t$. Therefore, for each $\tilde{r}_{ij}(0) \neq 0$, there exists $T_r = V(\tilde{r}_{ij}(0))/(\gamma l_{[0,t]})$ such that $V(\tilde{r}_{ij}(T_r)) = 0$, which proves the global and finite-time convergence. ∎

Remark 1. Although we require the excitation condition (21) to hold for all $t \geq 0$, it follows from the proof of Proposition 1 that, to guarantee the finite-time convergence, the excitation condition is only needed to hold on the time interval $[0, T_r]$. The difference is that the PE condition (21) guarantees not only the finite-time convergence but also the *stability* for the error system (22). In fact, the the function $V(\tilde{r}_{ij})$ is a weak Lyapunov function because $\dot{V} \leq 0$, which shows that the system (22) is *globally bounded* and *locally Lyapunov stable*. Together with the PE condition (21), which guarantees the *global finite-time convergence*, we conclude that the system has global finite-time stability. In practical applications, to guarantee finite-time *convergence*, only the finite-time excitation condition is required, which is called the interval excitation (IE) condition. Given the initial estimation error $\tilde{r}_{ij}(0)$, the time T_r can be estimated *a priori*. Due to the finite-time convergence, users can implement the excitation condition in advance, and then, apply the control laws after T_r to avoid the transient.

Remark 2. In the design of the distributed range observer, only the *kinematic* equations of the vehicles are utilized to obtain (14) and (15). No kinetic equation is used in the design, and thus, the distributed sliding mode range observer is applicable to both fully-actuated and underactuated systems.

4 | FORMATION CONTROL DEVELOPMENT

4.1 | Desired attitude trajectory generation

Unlike fully-actuated systems, underactuated mechanical systems cannot be commanded to track arbitrary trajectories. To be more precise, for the 6-DOF spatial vehicle model (6) and (7) with two degrees of underactuation, the desired trajectories can only be independently specified for four configuration variables.[15] Considering the formation objective (8), in addition to controlling the three position variables, one attitude variable also can be independently controlled. The other two attitude variables must be determined from the constraints imposed due to underactuation.

The vehicle model (6) and (7) has three possible structural heterogeneities, which correspond to the three possible configurations of the thrust actuator, that is, $u_{\mathbf{i}} = [u_{x\mathbf{i}}, 0, 0]^\top, [0, u_{y\mathbf{i}}, 0]^\top$, or $[0, 0, u_{z\mathbf{i}}]^\top$. Introducing a virtual input $\nu_{\mathbf{i}} = [\nu_{x\mathbf{i}}, \nu_{y\mathbf{i}}, \nu_{z\mathbf{i}}]^\top \in \mathbb{R}^3$ in the position dynamics, we have

$$\ddot{\xi}_{\mathbf{i}} = \nu_{\mathbf{i}} + g_{\mathbf{i}}(\eta_{\mathbf{i}}, u_{\mathbf{i}}, \dot{\xi}_{\mathbf{i}}, \nu_{\mathbf{i}}), \tag{25}$$

where $g_{\mathbf{i}}(\eta_{\mathbf{i}}, u_{\mathbf{i}}, \dot{\xi}_{\mathbf{i}}, \nu_{\mathbf{i}}) = R(\eta_{\mathbf{i}})u_{\mathbf{i}} + G_{\mathbf{i}}/m_{\mathbf{i}} - D_{\bar{\xi}\mathbf{i}}(\eta_{\mathbf{i}})\dot{\xi}_{\mathbf{i}} - \nu_{\mathbf{i}}$. The desired attitude trajectory $\eta_{\mathbf{i}d}(t) = [\phi_{\mathbf{i}d}(t), \theta_{\mathbf{i}d}(t), \psi_{\mathbf{i}d}(t)]^\top$ and the thrust $u_{\mathbf{i}}(t)$ are selected such that $g_{\mathbf{i}}(\eta_{\mathbf{i}d}(t), u_{\mathbf{i}}(t), \dot{\xi}_{\mathbf{i}}, \nu_{\mathbf{i}}) = 0$, for all $t \geq 0$. Specifically, denoting $\mu_{\mathbf{i}} = [\mu_{x\mathbf{i}}, \mu_{y\mathbf{i}}, \mu_{z\mathbf{i}}]^\top = D_{\bar{\xi}\mathbf{i}}(\eta_{\mathbf{i}})\dot{\xi}_{\mathbf{i}} + \nu_{\mathbf{i}} - G_{\mathbf{i}}/m_{\mathbf{i}}$, the desired trajectories $\eta_{\mathbf{i}d}(t)$ and the thrust $u_{\mathbf{i}}(t)$ are selected such that $R(\eta_{\mathbf{i}d}(t))u_{\mathbf{i}}(t) = \mu_{\mathbf{i}}(t)$. Note that the signal $\mu_{\mathbf{i}}(t)$ is available. For the three cases, we propose the attitude resolution as follows:

Case 1. ($u_{\mathbf{i}} = [u_{x\mathbf{i}}, 0, 0]^\top$; $\phi_{\mathbf{i}}$ is independently controlled.) Given $\phi_{\mathbf{i}d}(t) = \phi_{\mathbf{i}}(t)$ and $\nu_{\mathbf{i}}(t)$, the thrust and desired attitude signals are selected as

$$u_{x\mathbf{i}} = \sqrt{\mu_{x\mathbf{i}}^2 + \mu_{y\mathbf{i}}^2 + \mu_{z\mathbf{i}}^2}, \tag{26}$$

$$\theta_{\mathbf{i}d} = \arcsin\left(-u_{x\mathbf{i}}^{-1}\mu_{z\mathbf{i}}\right), \tag{27}$$

$$\psi_{\mathbf{i}d} = \arctan\left(\mu_{x\mathbf{i}}^{-1}\mu_{y\mathbf{i}}\right). \tag{28}$$

Case 2. ($u_{\mathbf{i}} = [0, u_{y\mathbf{i}}, 0]^\top$; $\theta_{\mathbf{i}}$ is independently controlled.) Given $\theta_{\mathbf{i}d}(t) = \theta_{\mathbf{i}}(t)$ and $\nu_{\mathbf{i}}(t)$, the thrust and desired attitude signals are selected as

$$u_{y\mathbf{i}} = \sqrt{\mu_{x\mathbf{i}}^2 + \mu_{y\mathbf{i}}^2 + \mu_{z\mathbf{i}}^2}, \tag{29}$$

$$\phi_{\mathbf{i}d} = \arcsin\left[\mu_{z\mathbf{i}}u_{y\mathbf{i}}^{-1}\sec(\theta_{\mathbf{i}d})\right], \tag{30}$$

$$\psi_{\mathbf{i}d} = \arccos\left[u_{y\mathbf{i}}\left(\mu_{x\mathbf{i}}\sin(\phi_{\mathbf{i}d})\sin(\theta_{\mathbf{i}d}) + \mu_{y\mathbf{i}}\cos(\phi_{\mathbf{i}d})\right)(\mu_{x\mathbf{i}}^2 + \mu_{y\mathbf{i}}^2)^{-1}\right]. \tag{31}$$

Case 3. ($u_{\mathbf{i}} = [0, 0, u_{z\mathbf{i}}]^\top$; $\psi_{\mathbf{i}}$ is independently controlled.) Given $\psi_{\mathbf{i}d}(t) = \psi_{\mathbf{i}}(t)$ and $\nu_{\mathbf{i}}(t)$, the thrust and desired attitude signals are selected as

$$u_{z\mathbf{i}} = \sqrt{\mu_{x\mathbf{i}}^2 + \mu_{y\mathbf{i}}^2 + \mu_{z\mathbf{i}}^2}, \tag{32}$$

$$\phi_{\mathbf{i}d} = \arcsin\left[u_{z\mathbf{i}}^{-1}\left(\mu_{x\mathbf{i}}\sin(\psi_{\mathbf{i}d}) - \mu_{y\mathbf{i}}\cos(\psi_{\mathbf{i}d})\right)\right], \tag{33}$$

$$\theta_{\mathbf{i}d} = \arctan\left[\mu_{z\mathbf{i}}^{-1}\left(\mu_{x\mathbf{i}}\cos(\psi_{\mathbf{i}d}) + \mu_{y\mathbf{i}}\sin(\psi_{\mathbf{i}d})\right)\right]. \tag{34}$$

Remark 3. Note that the position subsystem (25) and the attitude subsystem (7) form a cascaded structure. That is, the (double-integrator) attitude subsystem (7) is decoupled from (25), and is controlled independently

by $\tilde{\tau}_{\mathbf{i}}$. Due to the simple double-integrator dynamics of (7), it is trivial to design control law $\tilde{\tau}_{\mathbf{i}}$ such that $|\eta_{\mathbf{i}}(t) - \eta_{\mathbf{i}d}(t)| \to 0$ as $t \to +\infty$. If the thrust $u_{\mathbf{i}}$ and $\eta_{\mathbf{i}d}(t)$ are selected as above, the interconnection term $g_{\mathbf{i}}(\eta_{\mathbf{i}}(t), u_{\mathbf{i}}, \dot{\xi}_{\mathbf{i}}, \nu_{\mathbf{i}})$ in (25) also tends to zero as $|\eta_{\mathbf{i}}(t) - \eta_{\mathbf{i}d}(t)| \to 0$. Then, the position subsystem (25) reduces to the double-integrator dynamics $\ddot{\xi}_{\mathbf{i}} = \nu_{\mathbf{i}}$, and the position control input $\nu_{\mathbf{i}}$ can be independently designed. The attitude resolution **Case 3** is frequently used in the quadrotor control design.[23,24,38]

4.2 | Generalized Slotine-Li controller

As shown in Remark 3, the control objective is to design the virtual control law $\nu_{\mathbf{i}}$ and input $\tilde{\tau}_{\mathbf{i}}$ for double-integrator dynamics to achieve the formation. It should be pointed out that the extension of consensus tracking algorithms from single-integrator dynamics to higher-order dynamics is nontrivial. Lemma 1 shows that switching topologies do *not* matter for single-integrator systems when the graph contains a spanning tree. However, for higher-order systems, the situation is radically different. For example, even under the time-invariant topology case, the controller parameters need to be selected carefully to achieve the consensus for double-integrator dynamics.[1] Under switching topology, the analysis becomes more complicated. In this section, we present the generalized Slotine-Li control strategy for *arbitrary order integrator dynamics* to solve the consensus tracking problem subject to switching topologies. The main idea of the generalized Slotine-Li control strategy is to find a new set of coordinates such that the consensus tracking problem for a higher-order system is converted into the consensus tracking problem for single-integrator dynamics in the new coordinates.

In Reference 34, an adaptive scheme (a.k.a. Slotine-Li controller) was proposed for trajectory tracking control of fully-actuated EL systems with unknown parameters. The main idea of the Slotine-Li controller is to introduce a virtual "reference velocity", and then, PD feedback is employed to steer the velocity variable to the "reference velocity". For illustration, consider the double-integrator dynamics $\ddot{x} = u$. The objective is to design a feedback u such that $x(t)$ tracks the desired trajectory $x_d(t)$. To this end, define the reference velocity $z = \dot{x}_d - (x - x_d)$ and the "sliding variable" $s = \dot{x} - z$. It is clear that if $s(t) \to 0$ as $t \to \infty$ (i.e., the velocity $\dot{x}(t)$ converges to the reference velocity $z(t)$), then the position error $x(t) - x_d(t)$ also converges to zero. That is, the tracking control problem for the second-order system is reduced to the stabilization problem of a first-order system, that is, $\dot{s} = u - \dot{z}$. This objective can be achieved by simply choosing the control $u = \dot{z} - ks$ with $k > 0$.

The Slotine-Li controller also can be used to solve the consensus tracking problem for multi-agent systems. Consider N double-integrator systems, that is, $\ddot{x}_{\mathbf{i}} = u_{\mathbf{i}}$ with $x_{\mathbf{i}} \in \mathbb{R}^n$, $\mathbf{i} = 1, \ldots, N$. Define the reference velocity, the sliding variable, and the control input as

$$\begin{cases} z_{\mathbf{i}} = \frac{1}{\sum_{\mathbf{j}\in\mathcal{N}_{\mathbf{i}}} a_{\mathbf{ij}}} \sum_{\mathbf{j}\in\mathcal{N}_{\mathbf{i}}} a_{\mathbf{ij}} \left[\dot{x}_{\mathbf{j}} - (x_{\mathbf{i}} - x_{\mathbf{j}})\right], \\ s_{\mathbf{i}} = \dot{x}_{\mathbf{i}} - z_{\mathbf{i}}, \\ u_{\mathbf{i}} = \dot{z}_{\mathbf{i}} - k_{\mathbf{i}} s_{\mathbf{i}}, \end{cases} \tag{35}$$

where $a_{\mathbf{ij}}$ and $\mathcal{N}_{\mathbf{i}}$ are defined in Section 2.3; $k_{\mathbf{i}} > 0$ is a constant control gain. Noting that the control law $u_{\mathbf{i}} = \dot{z}_{\mathbf{i}} - k_{\mathbf{i}} s_{\mathbf{i}}$ guarantees that $s_{\mathbf{i}}(t) \to 0$ exponentially, and on the sliding manifold $\{s_{\mathbf{i}} \equiv 0\}$, the closed-loop dynamics are given by

$$\dot{x}_{\mathbf{i}} = \frac{1}{\sum_{\mathbf{j}\in\mathcal{N}_{\mathbf{i}}} a_{\mathbf{ij}}} \sum_{\mathbf{j}\in\mathcal{N}_{\mathbf{i}}} a_{\mathbf{ij}} \left[\dot{x}_{\mathbf{j}} - (x_{\mathbf{i}} - x_{\mathbf{j}})\right]. \tag{36}$$

The first-order dynamics (36) are exactly the same as (9), and thus, it follows from Lemma 1 that the consensus tracking problem is solved if the communication topology contains a directed spanning tree. In summary, the closed-loop system on the sliding manifold $\{s_{\mathbf{i}} \equiv 0\}$ recovers the classical single-integrator consensus tracking algorithm.

The algorithm (35) works well when the communication topology is fixed. However, it has a fatal flaw when the topology is dynamically changing. For instance, under switching topologies, $a_{\mathbf{ij}}(t)$ and the reference velocity $z_{\mathbf{i}}(t)$ are no longer continuous. Thus, the control law $u_{\mathbf{i}} = \dot{z}_{\mathbf{i}} - k_{\mathbf{i}} s_{\mathbf{i}}$ cannot be implemented because it involves the time derivative of a discontinuous term. To solve this problem, instead of defining the reference velocity $z_{\mathbf{i}}(t)$ as in (35), we define $z_{\mathbf{i}}(t)$ by

integration. Consider the following algorithm

$$\begin{cases} \dot{z}_{\mathbf{i}} = \frac{1}{\Xi_{\mathbf{i}}(t)} \sum_{\mathbf{j}\in\mathcal{N}_{\mathbf{i}}(t)} a_{\mathbf{ij}}(t) \left[\ddot{x}_{\mathbf{j}} - (\alpha+1)(\dot{x}_{\mathbf{i}} - \dot{x}_{\mathbf{j}}) - \alpha(x_{\mathbf{i}} - x_{\mathbf{j}})\right], \\ s_{\mathbf{i}} = \dot{x}_{\mathbf{i}} - z_{\mathbf{i}}, \\ u_{\mathbf{i}} = \dot{z}_{\mathbf{i}} - k_{\mathbf{i}} s_{\mathbf{i}}, \end{cases} \tag{37}$$

where $\alpha > 0$ is a control gain, and $\Xi_{\mathbf{i}}(t)$ is defined in (9). It should be pointed out that the reference velocity $z_{\mathbf{i}}(t)$ is differentiable due to the integration action, and thus, the control law $u_{\mathbf{i}} = \dot{z}_{\mathbf{i}} - k_{\mathbf{i}} s_{\mathbf{i}}$ is well defined. The control law $u_{\mathbf{i}} = \dot{z}_{\mathbf{i}} - k_{\mathbf{i}} s_{\mathbf{i}}$ ensures that $s_{\mathbf{i}}(t) \to 0$ (and $\dot{s}_{\mathbf{i}}(t) \to 0$) exponentially. Consider the closed-loop dynamics on the manifold $\{\dot{s}_{\mathbf{i}} \equiv 0\}$, which are given by

$$(\ddot{x}_{\mathbf{i}} + \alpha\dot{x}_{\mathbf{i}}) = \frac{1}{\Xi_{\mathbf{i}}(t)} \sum_{\mathbf{j}\in\mathcal{N}_{\mathbf{i}}(t)} a_{\mathbf{ij}}(t) \left\{(\ddot{x}_{\mathbf{j}} + \alpha\dot{x}_{\mathbf{j}}) - \left[(\dot{x}_{\mathbf{i}} + \alpha x_{\mathbf{i}}) - (\dot{x}_{\mathbf{j}} + \alpha x_{\mathbf{j}})\right]\right\}. \tag{38}$$

Note that the system (38) has the same structure as (9). It follows from Lemma 1 that $(\dot{x}_{\mathbf{i}} + \alpha x_{\mathbf{i}}) - (\dot{x}_{\mathbf{j}} + \alpha x_{\mathbf{j}}) \to 0$ as $t \to +\infty$, for all $\mathbf{i},\mathbf{j} \in \mathcal{V}$. Therefore, we have

$$(\dot{x}_{\mathbf{i}} - \dot{x}_{\mathbf{j}}) = -\alpha(x_{\mathbf{i}} - x_{\mathbf{j}}) + \epsilon_t, \quad \forall \mathbf{i},\mathbf{j} \in \mathcal{V}, \tag{39}$$

where $\epsilon_t \to 0$. It follows from the converging-input converging-state property of stable linear systems that $(x_{\mathbf{i}} - x_{\mathbf{j}}) \to 0$ as $t \to \infty$,[42] and thus, the consensus tracking problem is solved. It should be noted that, if the communication topology is fixed, that is, $a_{\mathbf{ij}}(t) \equiv a_{\mathbf{ij}}$ for all $\mathbf{i},\mathbf{j} \in \mathcal{V}$, then the control law (37) reduces to the Slotine-Li controller (35) when $\alpha = 0$.

This idea can be generalized to the m-th order integrator-chain model. The generalized Slotine-Li controller is given by

$$\begin{cases} z_{\mathbf{i}}^{(m-1)} = \frac{1}{\Xi_{\mathbf{i}}(t)} \sum_{j\in\mathcal{N}_{\mathbf{i}}(t)} a_{\mathbf{ij}}(t) \left[x_{\mathbf{j}}^{(m)} - (1+\alpha_{m-1})\left(x_{\mathbf{i}}^{(m-1)} - x_{\mathbf{j}}^{(m-1)}\right) - (\alpha_{m-1}+\alpha_{m-2})\left(x_{\mathbf{i}}^{(m-2)} - x_{\mathbf{j}}^{(m-2)}\right) - \cdots \right. \\ \qquad\qquad \left. \cdots - (\alpha_2+\alpha_1)(\dot{x}_{\mathbf{i}} - \dot{x}_{\mathbf{j}}) - \alpha_1(x_{\mathbf{i}} - x_{\mathbf{j}})\right], \\ s_{\mathbf{i}} = \dot{x}_{\mathbf{i}} - z_{\mathbf{i}}, \\ u_{\mathbf{i}} = z_{\mathbf{i}}^{(m-1)} - k_{1\mathbf{i}} s_{\mathbf{i}} - \cdots - k_{(m-1)\mathbf{i}} s_{\mathbf{i}}^{(m-2)}, \end{cases} \tag{40}$$

where the parameters $\alpha_1, \ldots, \alpha_{m-1}$ are chosen such that the matrix $A(\alpha_1, \ldots, \alpha_{m-1})$ is Hurwitz, $k_{1\mathbf{i}}, \ldots, k_{(m-1)\mathbf{i}}$ are chosen such that the matrix $A\left(k_{1\mathbf{i}}, \ldots, k_{(m-1)\mathbf{i}}\right)$ is Hurwitz, and the matrix $A(\cdot)$ is defined as

$$A(k_1, \ldots, k_{m-1}) = \begin{bmatrix} 0 & 1 & 0 & \cdots & 0 \\ 0 & 0 & 1 & \cdots & 0 \\ \vdots & \vdots & \vdots & \ddots & \vdots \\ 0 & 0 & 0 & \cdots & 1 \\ -k_1 & -k_2 & -k_3 & \cdots & -k_{m-1} \end{bmatrix} \in \mathbb{R}^{(m-1)\times(m-1)}. \tag{41}$$

Theorem 1. *Consider the m-th order integrator-chain model $x_{\mathbf{i}}^{(m)} = u_{\mathbf{i}}$, where $x_{\mathbf{i}} \in \mathbb{R}^n$, $\mathbf{i} = 1, \ldots, N$, and $m, n, N \in \mathbb{Z}_{>0}$. Then, under the generalized Slotine-Li controller (40), the consensus tracking problem is solved provided that Assumption 1 holds.*

Proof. Noting that the reference velocity $z_{\mathbf{i}}(t)$ is differentiable up to $(m-1)$-th order, we have

$$s_{\mathbf{i}}^{(m-1)} = x_{\mathbf{i}}^{(m)} - z_{\mathbf{i}}^{(m-1)}. \tag{42}$$

Substituting $x_{\mathbf{i}}^{(m)} = u_{\mathbf{i}}$ into (42) yields $s_{\mathbf{i}}^{(m-1)} = -k_{1\mathbf{i}}s_{\mathbf{i}} - \cdots - k_{(m-1)\mathbf{i}}s_{\mathbf{i}}^{(m-2)}$. The condition $A\left(k_{1\mathbf{i}}, \ldots, k_{(m-1)\mathbf{i}}\right)$ being Hurwitz implies that $\left(s_{\mathbf{i}}, \dot{s}_{\mathbf{i}}, \ldots, s_{\mathbf{i}}^{(m-1)}\right)(t) \to 0$ exponentially as $t \to +\infty$. On the other hand, substituting $z_{\mathbf{i}}^{(m-1)}$ into (42), and denoting $q_{\mathbf{i}} = x_{\mathbf{i}}^{(m-1)} + \alpha_{(m-1)}x_{\mathbf{i}}^{(m-2)} + \cdots + \alpha_2\dot{x}_{\mathbf{i}} + \alpha_1 x_{\mathbf{i}}$, we recover the first-order consensus algorithm

$$\dot{q}_{\mathbf{i}} = \frac{1}{\Xi_{\mathbf{i}}(t)} \sum_{\mathbf{j}\in\mathcal{N}_{\mathbf{i}}(t)} a_{\mathbf{ij}}(t)\left[\dot{q}_{\mathbf{j}} - \left(q_{\mathbf{i}} - q_{\mathbf{j}}\right)\right] + s_{\mathbf{i}}^{(m-1)}(t), \tag{43}$$

which can be viewed as an exponentially stable linear system (with respect to the equilibrium manifold $\{(x_{\mathbf{1}}, \ldots, x_{\mathbf{N}}) : x_{\mathbf{i}} = x_{\mathbf{j}}, \forall \mathbf{i},\mathbf{j} \in \mathcal{V}\}$)[1,43] with an exponentially decaying input $s_{\mathbf{i}}^{(m-1)}(t)$. It follows from Lemma 1 and the converging-input converging-state property for stable linear systems that the exponential consensus is achieved for variable $q_{\mathbf{i}}$.[42] That is, $|q_{\mathbf{i}}(t) - q_{\mathbf{j}}(t)| \to 0$ exponentially as $t \to +\infty$, for all $\mathbf{i},\mathbf{j} \in \mathcal{V}$. Finally, it follows from the condition $A(\alpha_1, \ldots, \alpha_{m-1})$ being Hurwitz that $|x_{\mathbf{i}}(t) - x_{\mathbf{j}}(t)| \to 0$ exponentially as $t \to +\infty$, for all $\mathbf{i},\mathbf{j} \in \mathcal{V}$, where the consensus tracking problem is solved under switching topologies. ■

Remark 4. Lemma 1 shows that switching topologies do not matter for single-integrator systems when the graph contains a spanning tree. However, as shown in Reference 1, the consensus tracking problem for double-integrator systems, let alone the m-th order integrator-chain, is far more complicated than single integrator systems, especially considering *directed* switching topologies.[5,43] The generalized Slotine-Li controller proposed in this section solves the consensus tracking problem under switching topologies for *arbitrary order* integrator-chain dynamics by reducing the closed-loop dynamics into the form of the first-order consensus system (43), and thus, switching topologies do not matter when the graph contains a spanning tree. It should be pointed out that $z_{\mathbf{i}}^{(m-1)}$ in (40) is derived from the linear consensus algorithm (9). It also can be generalized to other nonlinear forms by considering different first-order nonlinear consensus algorithms such as finite-time consensus protocol,[4] bounded control input consensus algorithm [Sec. 3.3.2],[1] and so forth. The control law $u_{\mathbf{i}}$ in (40) can also be generalized to other nonlinear forms. For example, the first-order sliding mode control law $u_{\mathbf{i}} = \dot{z}_{\mathbf{i}} - k_{\mathbf{i}}\text{sign}(s_{\mathbf{i}})$ guarantees $s_{\mathbf{i}}(t) \to 0$ in finite time and is robust to bounded match disturbances; or adaptive neural network control law can be used to compensate unknown dynamics.[44,45]

Remark 5. Another advantage of the first-order linear consensus algorithm (43) is, as shown in Reference 9 (Thm. 10.8), that under communication delays, for all $\mathbf{i},\mathbf{j} \in \mathcal{V}$, $|q_{\mathbf{i}}(t) - q_{\mathbf{j}}(t)|$ is uniformly ultimately bounded (UUB) no matter how large the communication delay is if the graph contains a spanning tree. Thus, a direct corollary from the proof of Theorem 1 is that, under communication delays, $|q_{\mathbf{i}}(t) - q_{\mathbf{j}}(t)|$ is UUB, and thus, $|x_{\mathbf{i}}(t) - x_{\mathbf{j}}(t)|$ is also UUB. That is, for the m-th order integrator-chain network, the generalized Slotine-Li algorithm (40) is robust to communication delays.

Remark 6. As shown in Theorem 1, the generalized Slotine-Li control strategy is applicable to m-th order integrator-chain model. It is well-known that, under full-state measurements, all fully-actuated systems can be feedback linearized into double-integrator dynamics, and then, the generalized Slotine-Li control strategy can be applied directly. However, it is impossible to use preliminary feedback to convert an *underactuated* system into the double-integrator dynamics. So the generalized Slotine-Li strategy may only be applied to a part of the system dynamics. For some underactuated systems with nonholonomic constraints, such as mobile robots and surface vessels, stabilization *cannot* be achieved by using continuous time-invariant state feedback due to the violation of Brockett's necessary condition. As a result, the generalized Slotine-Li strategy, which is essentially continuous time-invariant state feedback, may not be applicable to such systems.

4.3 | Formation control design

We apply the proposed finite-time sliding mode observer, attitude resolution, and the generalized Slotine-Li design to the formation control problem for heterogeneous spatial underactuated vehicle networks.

Position control design. Consider the position dynamics (25) and the finite-time sliding mode observer (19) and (20). We propose the following observer-based generalized Slotine-Li control law for $\nu_{\mathbf{i}}$

$$\begin{cases} \dot{\mathfrak{z}}_{1\mathbf{i}} = \frac{1}{\Xi_{\mathbf{i}}(t)} \sum\limits_{\mathbf{j}\in\mathcal{N}_{\mathbf{i}}(t)} a_{\mathbf{ij}}(t) \left[\ddot{\xi}_{\mathbf{j}} - (\alpha_1+1)(\dot{\xi}_{\mathbf{i}} - \dot{\xi}_{\mathbf{j}}) + \alpha_1 \left(R(\eta_{\mathbf{i}})\hat{\zeta}_{\mathbf{ij}} + d_{\mathbf{ij}}\right)\right], \\ s_{1\mathbf{i}} = \dot{\xi}_{\mathbf{i}} - \mathfrak{z}_{1\mathbf{i}}, \\ \nu_{\mathbf{i}} = \dot{\mathfrak{z}}_{1\mathbf{i}} - k_{1\mathbf{i}} s_{1\mathbf{i}}, \end{cases} \tag{44}$$

where $\alpha_1, k_{1\mathbf{i}} > 0$ are the control gains and $\hat{\zeta}_{\mathbf{ij}}(t)$ is the output of the sliding mode observer (19) and (20).

Attitude control design. Consider the attitude subsystem (7). It is clear that the attitude dynamics are decoupled and controlled by three independent control inputs, that is, $\tilde{\tau}_{\mathbf{i}} = [\tilde{\tau}_{\phi\mathbf{i}}, \tilde{\tau}_{\theta\mathbf{i}}, \tilde{\tau}_{\psi\mathbf{i}}]^\top$. For the three cases discussed in Section 4.1, we apply the generalized Slotine-Li control law to the independently controlled attitude variable. Specifically, for **Case 1**, $\phi_{\mathbf{i}}$ is independently controlled, and we propose

$$\begin{cases} \dot{\mathfrak{z}}_{2\mathbf{i}} = \frac{1}{\Xi_{\mathbf{i}}(t)} \sum\limits_{\mathbf{j}\in\mathcal{N}_{\mathbf{i}}(t)} a_{\mathbf{ij}}(t) \left[\ddot{\phi}_{\mathbf{j}} - (\alpha_2+1)(\dot{\phi}_{\mathbf{i}} - \dot{\phi}_{\mathbf{j}}) - \alpha_2 \left(\phi_{\mathbf{i}} - \phi_{\mathbf{j}}\right)\right], \\ s_{2\mathbf{i}} = \dot{\xi}_{\mathbf{i}} - \mathfrak{z}_{2\mathbf{i}}, \\ \tilde{\tau}_{\phi\mathbf{i}} = \dot{\mathfrak{z}}_{2\mathbf{i}} - k_{2\mathbf{i}} s_{2\mathbf{i}}, \end{cases} \tag{45}$$

where $\alpha_2, k_{2\mathbf{i}} > 0$ are the control gains. Then, the thrust $u_{\mathbf{i}}(t)$ and the other two desired attitude signals $(\theta_{\mathbf{i}d}(t), \psi_{\mathbf{i}d}(t))$ are given by (26)–(28). Given the desired trajectories $(\theta_{\mathbf{i}d}(t), \psi_{\mathbf{i}d}(t))$, the trajectory tracking control design is trivial for double-integrator $(\theta_{\mathbf{i}}, \psi_{\mathbf{i}})$-subsystems. Here, we choose the sliding mode control because of its simplicity and robustness

$$\tilde{\tau}_{\theta\mathbf{i}} = -\lambda_1 \dot{\tilde{\theta}}_{\mathbf{i}} - k_{3\mathbf{i}} \mathrm{sign}(s_{3\mathbf{i}}), \quad s_{3\mathbf{i}} = \dot{\tilde{\theta}}_{\mathbf{i}} + \lambda_1 \tilde{\theta}_{\mathbf{i}}, \tag{46}$$

$$\tilde{\tau}_{\psi\mathbf{i}} = -\lambda_2 \dot{\tilde{\psi}}_{\mathbf{i}} - k_{4\mathbf{i}} \mathrm{sign}(s_{4\mathbf{i}}), \quad s_{4\mathbf{i}} = \dot{\tilde{\psi}}_{\mathbf{i}} + \lambda_2 \tilde{\psi}_{\mathbf{i}}, \tag{47}$$

where $\tilde{\theta}_{\mathbf{i}} = \theta_{\mathbf{i}} - \theta_{\mathbf{i}d}$; $\tilde{\psi}_{\mathbf{i}} = \psi_{\mathbf{i}} - \psi_{\mathbf{i}d}$; and $\lambda_1 > 0$, $\lambda_2 > 0$, $k_{3\mathbf{i}} > \sup\{|\ddot{\theta}_{\mathbf{i}d}(t)|\}$, and $k_{4\mathbf{i}} > \sup\{|\ddot{\psi}_{\mathbf{i}d}(t)|\}$ are control gains. It should be pointed out that other control strategies such as linear PD+ controller or higher-order sliding mode controller also can be used to solve the trajectory tracking control problem. For **Case 2** and **Case 3**, replace the independently controlled attitude variable ϕ in (45) by θ and ψ, respectively; generate thrust and desired attitude signals using (29)–(31) and (32)–(34), respectively; and replace (θ, ψ) in (46) and (47) by (ϕ, ψ) and (ϕ, θ), respectively.

Theorem 2. *Consider the vehicle dynamics (25), (7). Suppose that Assumption 1 holds. Then, the controller (44)–(47), together with the finite-time sliding mode observer (19) and (20), solves the formation tracking problem.*

Proof. The vehicle dynamics (25), (7) is in the $(\xi_{\mathbf{i}}, \eta_{\mathbf{i}})$-cascaded structure. For the $\eta_{\mathbf{i}}$-subsystem, substituting (46) and (47) into (7), yields $\dot{s}_{3\mathbf{i}} = -k_{3\mathbf{i}}\mathrm{sign}(s_{3\mathbf{i}}) - \ddot{\theta}_{\mathbf{i}d}(t)$ and $\dot{s}_{4\mathbf{i}} = -k_{4\mathbf{i}}\mathrm{sign}(s_{4\mathbf{i}}) - \ddot{\psi}_{\mathbf{i}d}(t)$. Then, conditions $k_{3\mathbf{i}} > \sup\{|\ddot{\theta}_{\mathbf{i}d}(t)|\}$ and $k_{4\mathbf{i}} > \sup\{|\ddot{\psi}_{\mathbf{i}d}(t)|\}$ imply that $s_{3\mathbf{i}}(t) \to 0$ and $s_{4\mathbf{i}}(t) \to 0$ in finite time. On the sliding manifolds $\{s_{3\mathbf{i}} = 0\}$ and $\{s_{4\mathbf{i}} = 0\}$, we have $\dot{\tilde{\theta}}_{\mathbf{i}} = -\lambda_1 \tilde{\theta}_{\mathbf{i}}$, and $\dot{\tilde{\psi}}_{\mathbf{i}} = -\lambda_2 \tilde{\psi}_{\mathbf{i}}$, which implies that $\theta_{\mathbf{i}}(t) - \theta_{\mathbf{i}d}(t) \to 0$ and $\psi_{\mathbf{i}}(t) - \psi_{\mathbf{i}d}(t) \to 0$ exponentially as $t \to +\infty$, and thus, we conclude that $|\eta_{\mathbf{i}}(t) - \eta_{\mathbf{i}d}(t)| \to 0$ exponentially. In **Case 2**, we have $\phi_{\mathbf{i}}(t) - \phi_{\mathbf{i}d}(t) \to 0$ and $\psi_{\mathbf{i}}(t) - \psi_{\mathbf{i}d}(t) \to 0$ exponentially as $t \to +\infty$, and in **Case 3**, we have $\phi_{\mathbf{i}}(t) - \phi_{\mathbf{i}d}(t) \to 0$ and $\theta_{\mathbf{i}}(t) - \theta_{\mathbf{i}d}(t) \to 0$ exponentially as $t \to +\infty$. Therefore, the same conclusion $|\eta_{\mathbf{i}}(t) - \eta_{\mathbf{i}d}(t)| \to 0$ also can be obtained for both **Case 2** and **Case 3**. Furthermore, the interconnection term $g_{\mathbf{i}}(\eta_{\mathbf{i}}(t), u_{\mathbf{i}}(t), \dot{\xi}_{\mathbf{i}}(t), \nu_{\mathbf{i}}(t)) \to 0$ as $t \to +\infty$ as mentioned in Remark 3. Moreover, it follows from Proposition 1 that the finite-time sliding mode observer (19) and (20) guarantees the global finite-time convergence of $\hat{\zeta}_{\mathbf{ij}}(t) - \zeta_{\mathbf{ij}}(t) \to 0$. Thus, after a finite time T_r, $\hat{\zeta}_{\mathbf{ij}}(t) \equiv \zeta_{\mathbf{ij}}(t) \equiv R(\eta_{\mathbf{i}})^\top(\xi_{\mathbf{j}} - \xi_{\mathbf{i}})$. Replace $\hat{\xi}_{\mathbf{ij}}(t)$ with $\xi_{\mathbf{ij}}(t)$ in (44), which recovers the generalized Slotine-Li controller structure (37). Also note that the controller (45) is exactly the same as the generalized Slotine-Li controller (37). Therefore, it follows from Theorem 1 that $\phi_{\mathbf{i}}(t) - \phi_{\mathbf{j}}(t) \to 0$ as $t \to +\infty$. Note that the dynamics $\dot{s}_{1\mathbf{i}} = \ddot{\xi}_{\mathbf{i}} - \dot{\mathfrak{z}}_{1\mathbf{i}} = -k_{1\mathbf{i}} s_{1\mathbf{i}} + g_{\mathbf{i}}(\eta_{\mathbf{i}}(t), u_{\mathbf{i}}(t), \dot{\xi}_{\mathbf{i}}(t), \nu_{\mathbf{i}}(t))$ can be viewed as a stable linear system with an input term $g_{\mathbf{i}}$, and the last term $g_{\mathbf{i}}(\eta_{\mathbf{i}}(t), u_{\mathbf{i}}(t), \dot{\xi}_{\mathbf{i}}(t), \nu_{\mathbf{i}}(t)) \to 0$ as

$t \to +\infty$. The converging-input converging-state property of linear systems implies that $s_{1\mathbf{i}}(t) \to 0$.[42] Finally, it follows from Theorem 1 that the control objective (8) is achieved, which completes the proof. ∎

In contrast to existing robust control methods for underactuated systems in the literature, such as the neuroadaptive controller in References 44,45, where the error converges to zero under bounded model uncertainties, we do not *explicitly* consider model uncertainties. Although any first-order consensus algorithm can be used, in this paper, we choose the first-order *linear* consensus algorithm (9) for simplicity, which guarantees *asymptotic* convergence of the formation error under switching topologies, and guarantees *bounded* formation error under bounded uncertainties, disturbances, and time delays. However, in order to achieve *asymptotic* convergence of the formation error under model uncertainties and disturbances, as claimed in Remark 4, the method also can be generalized to first-order *nonlinear* consensus algorithms.

5 | NUMERICAL SIMULATION

In this section, we apply the proposed range observer-based formation control strategy to a heterogeneous spatial underactuated vehicle network including one AUV and four quadrotor unmanned aerial vehicles (UAVs). We provide numerical simulation results to verify the performance of the proposed formation control law. All parameters are given in SI units.

The four quadrotors are numbered **1** to **4** and the AUV is agent **5**. Note that the model of the AUV can be classified into **Case 1** and the model of quadrotors can be classified into **Case 3**.

We assume that the desired formation shape is an inverted quadrangular pyramid. Specifically, the desired formation shape of the group of quadrotors is a horizontal square with the leader vehicle **1** located at its upper-left corner, as shown in Figure 3. The length of the square sides is 5 m. The desired XY position of the AUV **5** is the center of the square in the formation, and the desired vertical position is 15 m lower than the horizontal square. In the simulation, the group leader is commanded to follow a circle of radius 1 m centered at $(0, 0, 10)$ and a constant speed of 1 rad/s. The desired yaw angle for the leader vehicle is 1 rad. The quadrotor parameters are selected as: $m_{\mathbf{i}} = 1$ kg, $I_{\mathbf{i}} = \text{diag}\{0.0127, 0.0125, 0.0227\}$ kg $\cdot$ m ^{2}, $D_{v\mathbf{i}} = \text{diag}\{0, 0, 0\}$, $D_{\omega\mathbf{i}} = \text{diag}\{0, 0, 0\}$ for $\mathbf{i} = \mathbf{1}, \ldots, \mathbf{4}$. The AUV parameters are selected as: $m_{\mathbf{5}} = 11.85$ kg, $I_{\mathbf{5}} = \text{diag}\{0.26, 2.51, 0.27\}$ kg $\cdot$ m ^{2}, $D_{v\mathbf{5}} = \text{diag}\{0.85, 3.11, 0.24\}$, $D_{\omega\mathbf{5}} = \text{diag}\{0.01, 1.61, 1.28\}$. The buoyancy force of the AUV is 114.2 N. The gravity acceleration $g = 9.81$ kg/s ^{2}. All vehicles start from rest at the initial positions shown in Figure 4 and the initial Euler angles are 0. The directed communication graph $\mathcal{G}(t)$ switches every 5 seconds from $\mathcal{G}_{(1)}$ to $\mathcal{G}_{(2)}$ to $\mathcal{G}_{(3)}$ and to $\mathcal{G}_{(4)}$, as shown in Figure 3. The components of the adjacency matrix are $a_{\mathbf{ij}}(t) = 1$ if $(\mathbf{j}, \mathbf{i}) \in \mathcal{E}(t)$ and $a_{\mathbf{ij}}(t) = 0$ otherwise.

The observer parameters in the simulation are selected as $\alpha = 5$ and $\gamma = 5$. The control parameters for the four quadrotors are selected as $k_{1\mathbf{i}} = 3$, $k_{2\mathbf{i}} = 3$, $k_{3\mathbf{i}} = 20$, $k_{4\mathbf{i}} = 20$ for $\mathbf{i} = 1, \ldots, 4$, $\alpha_1 = 2$, $\alpha_2 = 3$, $\lambda_1 = 3$, $\lambda_2 = 3$. The control parameters for the AUV are selected as: $k_{1\mathbf{5}} = 2$, $k_{2\mathbf{5}} = 2$, $k_{3\mathbf{5}} = 25$, $k_{4\mathbf{5}} = 25$, $\alpha_1 = 1$, $\alpha_2 = 1$, $\lambda_1 = 5$, $\lambda_2 = 5$. To avoid excessive chattering, we used the hyperbolic tangent function tanh to approximate the discontinuous signum function.

Simulation results are illustrated in Figures 4,5,6, and 7. Figure 4 shows the paths of all five vehicles in three-dimensional space and the XY plane (i.e., the top view) with the formation illustrated at $t = 20$ s. Figure 5 shows the time history of the configuration errors of the five vehicles in the formation, where $\xi_{\mathbf{i}d} = [x_{\mathbf{i}d}, y_{\mathbf{i}d}, z_{\mathbf{i}d}]^\top = (1/\Xi_{\mathbf{i}}(t)) \sum_{\mathbf{j} \in \mathcal{N}_{\mathbf{i}}(t)} a_{\mathbf{ij}}(t)(\xi_{\mathbf{j}} + d_{\mathbf{ij}})$. It can be seen from Figure 5 that the convergence is exponential and the formation is achieved after about 6 s. Figure 6 shows the time history of the Euler angles of the five vehicles in the formation. The yaw angles of all four quadrotors are in consensus and converge to the desired angle (1 rad). The roll angle of the AUV converges to the desired trajectory assigned by the quadrotors, while its yaw angle linearly increases as time tends to

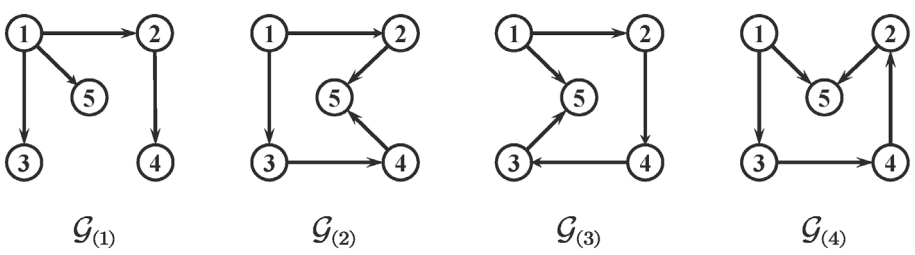

FIGURE 3 Directed switching topologies in the numerical simulation.

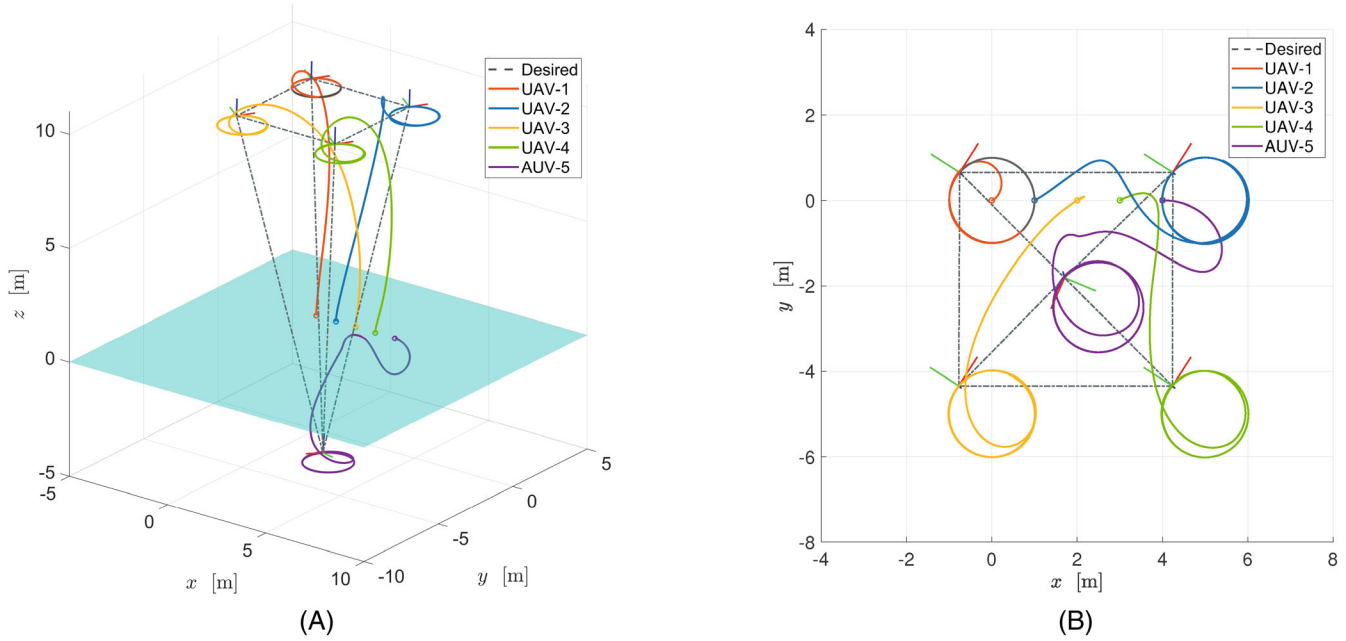

FIGURE 4 The trajectories of the five vehicles in three-dimensional space (left) and the top view (right).

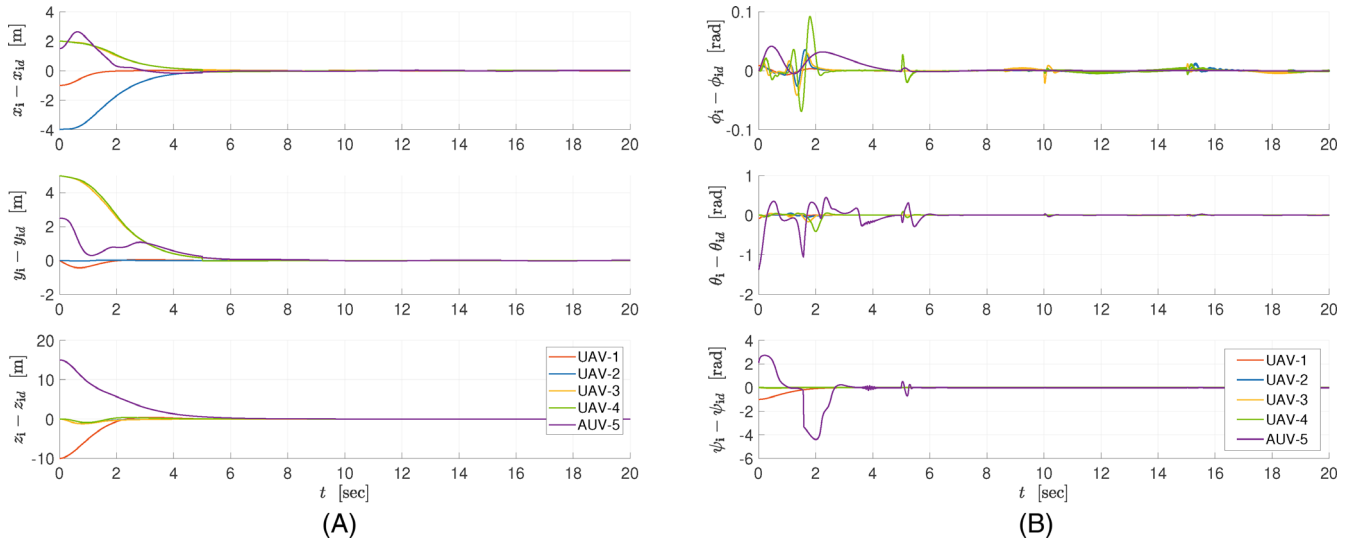

FIGURE 5 Time history of the configuration errors of the five vehicles in the formation: Position errors (left), attitude errors (right).

infinity due to continuous rotation around its circular path. It is noted that all the roll and pitch angles are in the interval $(-\pi/2, \pi/2)$. The estimation errors of the range observers for the four follower vehicles are shown in Figure 7. It can be seen that the convergence is achieved in finite time, and the estimated ranges converge to the actual ranges in 4 s. It can be clearly seen from the two subfigures in Figure 7 that the estimation error occurs at the switching moment. This is reasonable because, at the switching moment, the leader of the follower vehicle changes from one to another. This estimation error is due to that during the transient phase, the formation error is not zero. However, as the formation error converges to zero, switching topologies will not influence the estimation, as shown in Figure 7. The numerical simulation demonstrates the effectiveness and robustness of the proposed formation controller under switching communication topologies. Figure 8 shows the control inputs of the five vehicles in formation. It can be seen from Figure 8A that the generalized Slotine-Li control laws $F_{z\mathbf{i}}$ and $\tilde{\tau}_{\psi\mathbf{i}}$ of the four UAVs are very smooth under switching topologies. The other two control inputs $\tilde{\tau}_{\phi\mathbf{i}}$ and $\tilde{\tau}_{\theta\mathbf{i}}$ have some shaking at the switching moments because only trivial sliding mode control laws are

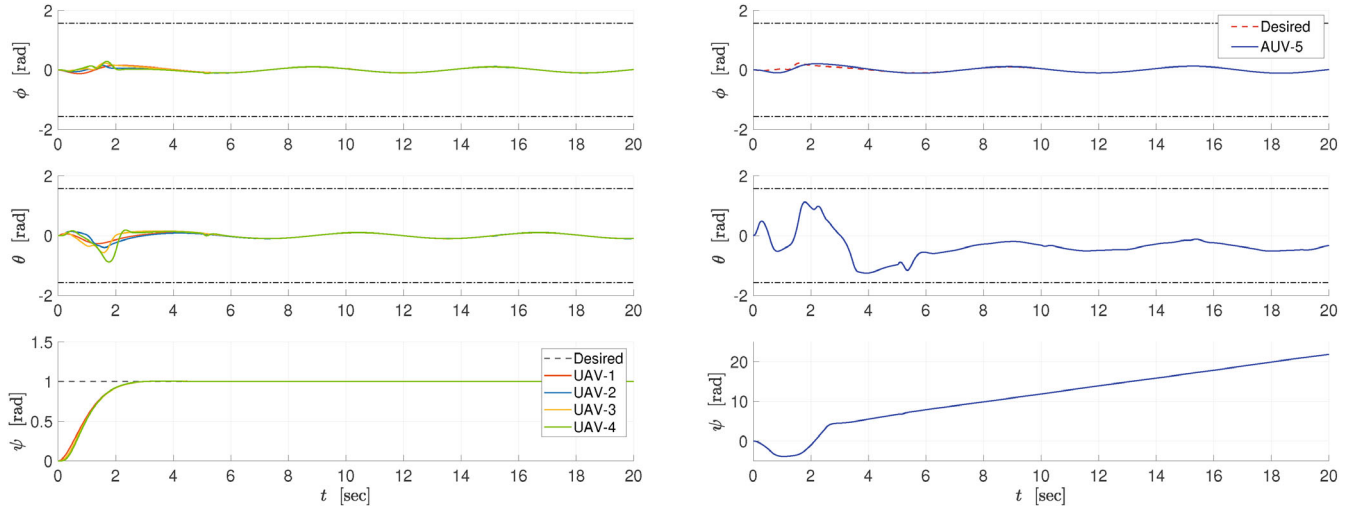

FIGURE 6 Time history of the Euler angles of the five vehicles in the formation; UAVs (left), AUV (right).

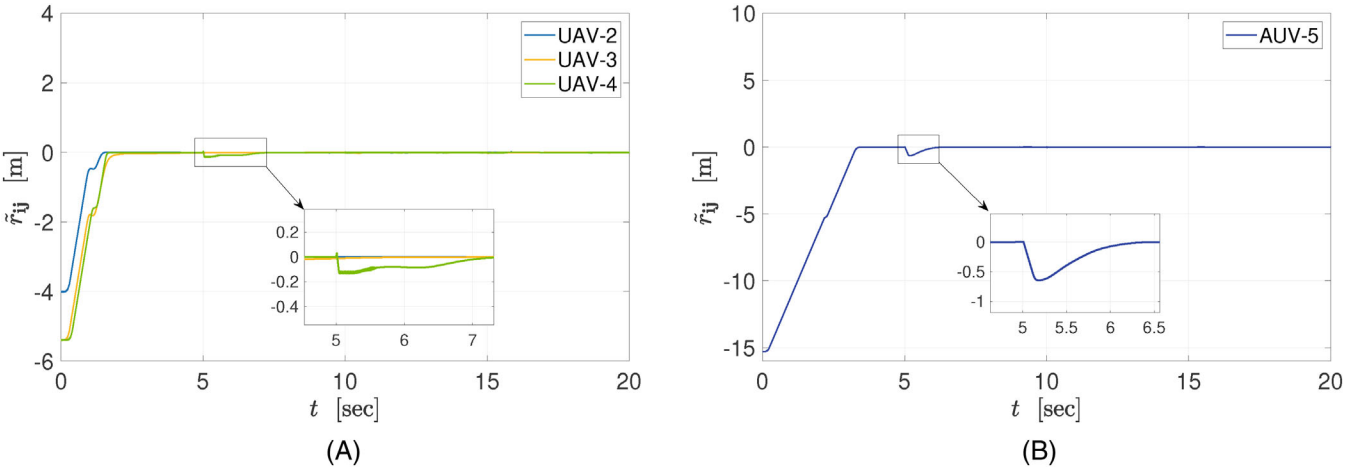

FIGURE 7 Time history of the estimation errors of the finite-time range observers; follower UAVs (left), AUV (right).

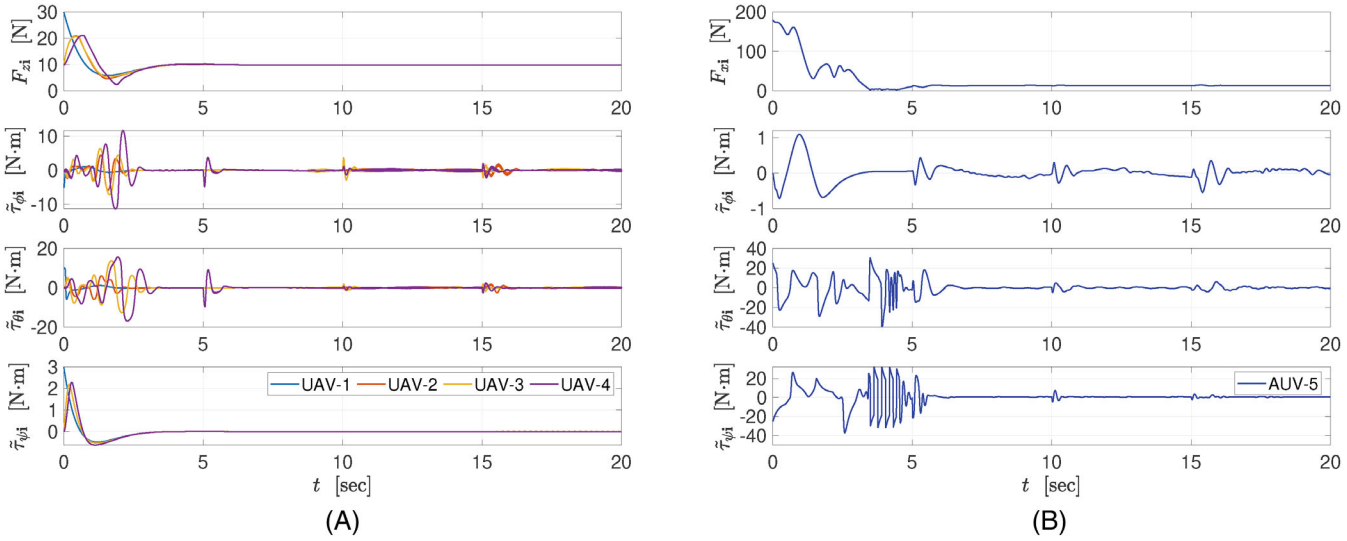

FIGURE 8 Time history of the four control inputs of the five vehicles in formation; UAVs (left), AUV (right).

applied. Figure 8B shows the inputs of the AUV, and the shaking of the generalized Slotine-Li control laws $F_{x\mathbf{i}}$ and $\tilde{\tau}_{\phi\mathbf{i}}$ at the switching moments is due to its leaders.

Remark 7. It can be seen from the proof of Proposition 1 that the parameter $\gamma > 0$ determines the convergence time T_r of the observer. That is, the larger γ, the quicker convergence of the observer. In practice, the two observer parameters α and γ are suggested to be selected moderately in order to avoid aggressive transient. Furthermore, the control parameters $k_{1\mathbf{i}}, k_{2\mathbf{i}}, \lambda_1$, and λ_2 determine the speed that trajectories converge to the sliding surface, and are also suggested to be selected moderately in order to avoid overshooting. The parameters α_1 and α_2 are usually selected as small values to guarantee the transient performance. Finally, the parameters $k_{3\mathbf{i}}, k_{4\mathbf{i}}$ are gains of sliding mode control, which are suggested to be chosen larger to guarantee robustness.

6 | CONCLUSIONS

The formation control problem for a team of heterogeneous spatial underactuated vehicles subject to switching topologies and communication delays has been addressed without requiring any relative position measurements. The spatial vehicle model is assumed to have two degrees of underactuation, which include underwater vehicles and quadrotors. A distributed sliding mode observer is used to estimate ranges between vehicles in finite time based on bearing angles, vehicle attitude, and local velocity measurements. Then, a distributed controller is presented to deal with switching communication topologies. Global asymptotic convergence is proved for the closed-loop system based on the cascaded structure of the vehicle systems. The simulation results show the effectiveness of the proposed formation control law. Future work will focus on the formation control of heterogeneous networks containing both planar and spatial vehicles. Furthermore, it will be interesting to apply the proposed control strategy to other distributed control and optimization problems for higher-order multi-agent systems such as containment control, distributed optimization[46] and distributed filtering[47] problems.

ACKNOWLEDGMENTS

This research was supported in part by the Office of Naval Research under grant N00014-19-1-2255.

CONFLICT OF INTEREST STATEMENT

The authors declare no potential conflict of interest.

ORCID

Bo Wang https://orcid.org/0000-0001-6047-1400
Sergey Nersesov https://orcid.org/0000-0003-0331-1181
Hashem Ashrafiuon https://orcid.org/0000-0001-5067-9064

REFERENCES

1. Ren W, Beard RW. *Distributed Consensus in Multi–Vehicle Cooperative Control*. Springer; 2008.
2. Olfati-Saber R, Murray RM. Consensus problems in networks of agents with switching topology and time-delays. *IEEE Trans. Automat. Contr.* 2004;49(9):1520-1533.
3. Ren W, Beard RW. Consensus seeking in multiagent systems under dynamically changing interaction topologies. *IEEE Trans. Automat. Contr.* 2005;50(5):655-661.
4. Xiao F, Wang L, Chen J, Gao Y. Finite-time formation control for multi-agent systems. *Automatica*. 2009;45(11):2605-2611.
5. Ren W. On Consensus Algorithms for Double-Integrator Dynamics. *IEEE Trans. Automat. Contr.* 2008;53(6):1503-1509.
6. Qin J, Gao H, Zheng WX. Second-order consensus for multi-agent systems with switching topology and communication delay. *Syst. Control Lett.* 2011;60(6):390-397.
7. Ren W. Distributed leaderless consensus algorithms for networked Euler–Lagrange systems. *Int. J. Control*. 2009;82(11):2137-2149.
8. Mei J, Ren W, Ma G. Distributed coordinated tracking with a dynamic leader for multiple Euler-Lagrange systems. *IEEE Trans. Automat. Contr.* 2011;56(6):1415-1421.
9. Ren W, Cao Y. *Distributed Coordination of Multi-Agent Networks: Emergent Problems, Models, and Issues*. Springer; 2011.
10. Zuo S, Song Y, Lewis FL, Davoudi A. Adaptive output formation-tracking of heterogeneous multi-agent systems using time-varying $\mathscr{L}_2$-gain design. *IEEE Control. Syst. Lett*. 2018;2(2):236-241.

11. Panteley E, Loría A. Synchronization and dynamic consensus of heterogeneous networked systems. *IEEE Trans. Automat. Contr.* 2017;62(8):3758-3773.
12. Oh KK, Park MC, Ahn HS. A survey of multi-agent formation control. *Automatica*. 2015;53:424-440.
13. Ashrafiuon H, Nersesov S, Clayton G. Trajectory tracking control of planar underactuated vehicles. *IEEE Trans. Automat. Contr.* 2016;62(4):1959-1965.
14. Fetzer KL, Nersesov S, Ashrafiuon H. Nonlinear control of three-dimensional underactuated vehicles. *Int. J. Robust Nonlinear Control.* 2020;30(4):1607-1621.
15. Fetzer KL, Nersesov SG, Ashrafiuon H. Trajectory tracking control of spatial underactuated vehicles. *Int. J. Robust Nonlinear Control.* 2021;31(10):4897-4916.
16. Jin X. Fault tolerant finite-time leader–follower formation control for autonomous surface vessels with LOS range and angle constraints. *Automatica*. 2016;68:228-236.
17. Yoo SJ, Park BS. Guaranteed performance design for distributed bounded containment control of networked uncertain underactuated surface vessels. *J. Frank Inst.* 2017;354(3):1584-1602.
18. Li S, Zhang J, Li X, Wang F, Luo X, Guan X. Formation control of heterogeneous discrete-time nonlinear multi-agent systems with uncertainties. *IEEE Trans. Ind. Electron.* 2017;64(6):4730-4740.
19. Wang B, Ashrafiuon H, Nersesov S. Leader–follower formation stabilization and tracking control for heterogeneous planar underactuated vehicle networks. *Syst. Control Lett.* 2021;156:105008.
20. Wang B, Nersesov S, Ashrafiuon H. Time–varying formation control for heterogeneous planar underactuated multi–vehicle systems. *J. Dyn. Syst. Meas. Control.* 2022;144(4):041006.
21. Wang B, Nersesov S, Ashrafiuon H. Robust formation control and obstacle avoidance for heterogeneous underactuated surface vessel networks. *IEEE Trans. Control Netw. Syst*. 2022;9(1):1.
22. Do KD. Coordination control of quadrotor VTOL aircraft in three-dimensional space. *Int. J. Control*. 2015;88(3):543-558.
23. Du H, Zhu W, Wen G, Duan Z, Lü J. Distributed formation control of multiple quadrotor aircraft based on nonsmooth consensus algorithms. *IEEE Trans. Cybern.* 2019;49(1):342-353.
24. Dou L, Yang C, Wang D, Tian B, Zong Q. Distributed finite-time formation control for multiple quadrotors via local communications. *Int. J. Robust Nonlinear Control*. 2019;29(16):5588-5608.
25. Liu H, Wang Y, Lewis FL, Valavanis KP. Robust formation tracking control for multiple quadrotors subject to switching topologies. *IEEE Trans. Control Netw. Syst.* 2020;7(3):1319-1329.
26. Restrepo E, Loria A, Sarras I, Marzat J. Robust consensus of high-order systems under output constraints: Application to rendezvous of underactuated UAVs. *IEEE Trans. Automat. Contr.* 2022;68(1):1.
27. Jin XZ, Che WW, Wu ZG, Deng C. Robust adaptive general formation control of a class of networked quadrotor aircraft. *IEEE Trans. Syst. Man Cybern: Syst*. 2022;52(12):7714-7726.
28. Shojaei K. Neural network formation control of underactuated autonomous underwater vehicles with saturating actuators. *Neurocomput*. 2016;194:372-384.
29. Wang J, Wang C, Wei Y, Zhang C. Filter-backstepping based neural adaptive formation control of leader-following multiple AUVs in three dimensional space. *Ocean Eng.* 2020;201:107150.
30. Zhang Y, Wang X, Wang S, Tian X. Three-dimensional formation–containment control of underactuated AUVs with heterogeneous uncertain dynamics and system constraints. *Ocean Eng.* 2021;238:109661.
31. Mu B, Zhang K, Shi Y. Integral sliding mode flight controller design for a quadrotor and the application in a heterogeneous multi-agent system. *IEEE Trans. Ind. Electron.* 2017;64(12):9389-9398.
32. Mu B, Shi Y. Distributed LQR consensus control for heterogeneous multiagent systems: Theory and experiments. *IEEE ASME Trans. Mechatron.* 2018;23(1):434-443.
33. Wang N, Ahn CK. Coordinated trajectory-tracking control of a marine aerial-surface heterogeneous system. *IEEE ASME Trans. Mechatron.* 2021;26(6):3198-3210.
34. Slotine JJ, Li W. On the adaptive control of robot manipulators. *Int. J. Rob. Res.* 1987;6(3):49-59.
35. Zhao S, Li Z, Ding Z. Bearing-only formation tracking control of multiagent systems. *IEEE Trans. Automat. Contr.* 2019;64(11):4541-4554.
36. Li Z, Tnunay H, Zhao S, Meng W, Xie SQ, Ding Z. Bearing-only formation control with prespecified convergence time. *IEEE Trans. Cybern*. 2020;52(1):620-629.
37. Wu K, Hu J, Lennox B, Arvin F. Finite-time bearing-only formation tracking of heterogeneous mobile robots with collision avoidance. *IEEE Trans. Circuits Syst. II Express Briefs*. 2021;68(10):3316-3320.
38. Carrillo LRG, López AED, Lozano R, Pégard C. *Quad Rotorcraft Control: Vision-based Hovering and Navigation*. Springer Science & Business Media; 2012.
39. Sastry S, Bodson M. *Adaptive Control: Stability, Convergence, and Robustness*. Prentice-Hall; 1989.
40. Hamel T, Samson C. Position estimation from direction or range measurements. *Automatica*. 2017;82:137-144.
41. Yi B, Jin C, Manchester IR. Globally convergent visual-feature range estimation with biased inertial measurements. *Automatica*. 2022;146:110639.
42. Desoer CA, Vidyasagar M. *Feedback Systems: Input-Output Properties*. SIAM; 1975.
43. Panteley E, Loria A, Sukumar S. Strict Lyapunov functions for consensus under directed connected graphs. *Proc. Euro. Control Conf*., IEEE. 2020 935–940.

44. Yang T, Sun N, Fang Y. Neuroadaptive control for complicated underactuated systems with simultaneous output and velocity constraints exerted on both actuated and unactuated states. *IEEE Trans. Neural Netw. Learn. Syst*. 2021. doi:10.1109/TNNLS.2021.3115960
45. Yang T, Chen H, Sun N, Fang Y. Adaptive neural network output feedback control of uncertain underactuated systems with actuated and unactuated state constraints. *IEEE Trans. Syst. Man Cybern: Syst*. 2021;52(11):7027-7043.
46. An W, Zhao P, Liu H, Hu J. Distributed multi-step subgradient projection algorithm with adaptive event-triggering protocols: a framework of multiagent systems. *Int. J. Syst. Sci.* 2022;53(13):2758-2772.
47. Song H, Ding D, Dong H, Yi X. Distributed filtering based on Cauchy-kernel-based maximum correntropy subject to randomly occurring cyber-attacks. *Automatica*. 2022;135:110004.

How to cite this article: Wang B, Nersesov S, Ashrafiuon H. Range observer-based formation control for heterogeneous spatial underactuated vehicle networks. *Int J Adapt Control Signal Process*. 2023;37(6):1492-1510. doi: 10.1002/acs.3585